United States Department of the Interior
Geological Survey

SHALLOW HYDROTHERMAL REGIME OF THE EAST BRAWLEY AND GLAMIS KNOWN GEOTHERMAL RESOURCE AREAS, SALTON TROUGH, CALIFORNIA

by

C.W. Mase, J.H. Sass, C.A. Brook, and Robert J. Munroe

Open-File Report 81-834
1981

Table of Contents

Abstract

Thermal gradients and thermal conductivities were obtained in real time using an in situ heat-flow technique in 15 shallow (90-150 m) wells drilled between Brawley and Glamis in the Imperial Valley, Southern California. The in situ measurements were supplemented by follow-up conventional temperature logs in seven of the wells and by laboratory measurements of thermal conductivity on drill cuttings. The deltaic sedimentary material comprising the upper ~100 m of the Salton Trough generally is poorly sorted and high in quartz resulting in quite high thermal conductivities (averaging 2.0 $Wm^{-1} K^{-1}$ as opposed to 1.2 to 1.7 for typical "alluvium"). A broad heat-flow anomaly with maximum of about 200 mWm^{-2} (~5 HFU) is centered between Glamis and East Brawley and is superimposed on a regional heat-flow high in excess of 100 mWm^{-2} (>2.5 HFU). The heat-flow high corresponds with a gravity maximum and partially with a minimum in electrical resistivity, suggesting the presence of a hydrothermal system at depth in this area.

INTRODUCTION

The East Brawley and Glamis KGRA's are located in the Imperial Valley, a subprovince of the Salton Trough, in southeastern California (Figure 1). The valley is situated at the southern end of the San Andreas fault system in a tectonic setting that is thought to involve a widely distributed shallow heat source. Evidence for hydrothermal activity is abundant throughout the Salton Trough region, which is generally considered as one of the major geothermal provinces of the world. Electrical production from the geothermal resources of the region currently stand at 170 MW (150 MW at Cerro Prieto and 10 MW each at Brawley and East Mesa).

During the latter part of 1980, the Conservation Division, U.S. Geological Survey, funded the Geothermal Studies Project, Geologic Division, to conduct a heat-flow study in a part of the Imperial Valley where shallow heat-flow data were not available. The purpose of this survey was to define the limits and magnitude of a suspected thermal anomaly and thereby support a KGRA classification (East Brawley). In an attempt to supply the necessary data, 15 wells ranging in depth from 90 to 150 meters were drilled and thermal conductivities, temperature gradients, and preliminary values of heat flow obtained in the field using the in situ heat-flow technique described by Sass and others (1981). Seven of the holes were cased for follow-up studies, and data from all wells were studied further to examine the relations among temperature gradients, in situ thermal conductivities, grain conductivities of drill cuttings and other geophysical quantities.

In this report, we review briefly the tectonic setting, geology, and previous heat flow and other geophysical studies for the region. The heat-flow data are then analyzed in terms of the regional hydrology and tectonics.

The following units are used throughout this report:

T, temperature, °C

K, thermal conductivity, 1 W $m^{-1}K^{-1}$ = 2.39 mcal $cm^{-1}s^{-1}°C^{-1}$

z, depth, m positive downwards

v_z, volume flux of water or vertical (seepage) velocity m s^{-1} or mm y^{-1}

Γ, vertical temperature gradient, °K km^{-1} = °C km^{-1}

q, vertical conductive heat flow mWm^{-2} = kW km^{-2}

or HFU (10^{-6} cal cm^{-2} s^{-1}): 1 HFU = 41.87 mWm^{-2}

Acknowledgment: We thank our colleague, Arthur H. Lachenbruch, for his helpful comments on the manuscript.

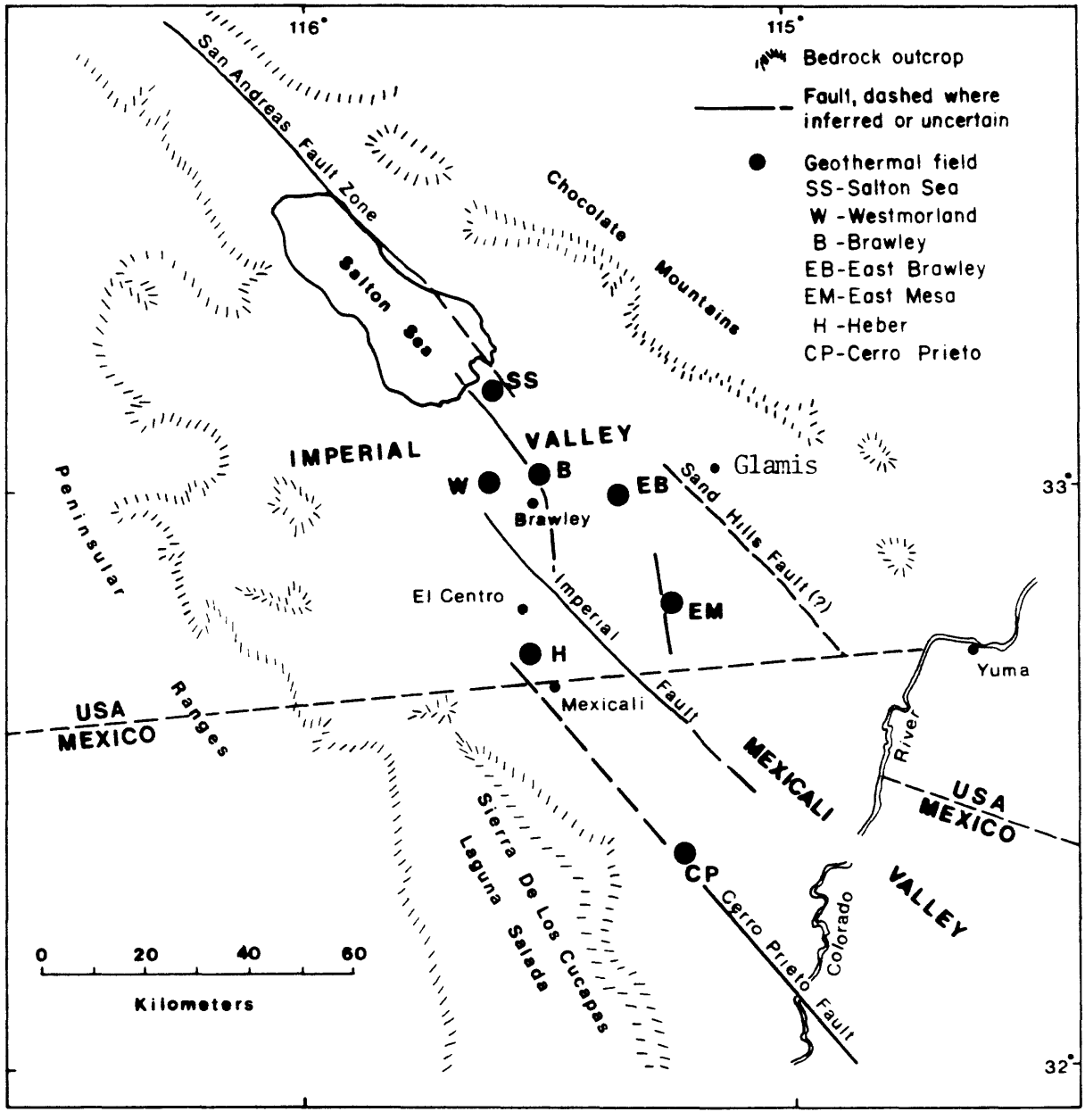

Figure 1. Map of the Imperial and Mexicali Valleys showing locations of known geothermal fields and selected faults.

GEOLOGIC SETTING

The East Brawley and Glamis KGRA's are situated within the Salton Trough, the sediment-filled landward extension of the Gulf of California. The Salton Trough and Gulf of California mark the transition from the divergent plate boundary of the East Pacific Rise to the transform plate boundary of the San Andreas fault system (Elders and others, 1972). The Salton Trough region is characterized by right-lateral strike-slip faulting, rapid tectonic extension and sedimentation, and patterns of high heat flow and seismicity, all of which combine to form a province favorable for the development of hydrothermal systems.

Elders and others (1972) propose the extension is in response to the opening of localized spreading centers occurring in the region of right-stepping offsets between active strands of right-lateral, strike-slip faults (commonly referred to as leaky transform faulting). Dilatation at these spreading centers is accompanied by the emplacement of basaltic to rhyolitic dikes and sills which account for the observed high heat flow and seismicity. Active local spreading centers are interpreted to occur in the vicinities of the Brawley, Salton Sea, and Cerro Prieto fields (Elders and others, 1972; Hill, 1977; Hill and others, 1975; Johnson and Hadley, 1976).

The Salton Trough is filled with late Tertiary and Quaternary clastic sediments. The sedimentary fill consists primarily of Pliocene to Holocene deltaic deposits derived from the Colorado River with coarser detritus along the margins derived from the adjacent mountain ranges (Muffler and Doe, 1968). Interbedded lacustrine deposits occur throughout the sedimentary fill, with Holocene muds and silts of ancient Lake Cahuilla forming the top 60 to 100 m of the stratigraphic section within the Imperial Valley (van de Kamp,

1973). Precambrian metamorphic rocks (mostly schist and gneiss), Mesozoic granitic rocks, and Miocene marine and continental clastic sedimentary rocks are exposed in the mountain ranges bounding the trough (Dibblee, 1954); however, it is not known if these rocks comprise the basement beneath the sedimentary fill of the trough. Fuis and others (1981) conclude from seismic velocity data that the sedimentary fill within the Imperial Valley consists of two main layers. The upper layer is interpreted as an unmetamorphosed sedimentary section 3.7 to 4.8 km thick, while the lower layer consists of a metamorphosed sedimentary "basement" that extends to depths of 10 to 16 km. A 1-km-thick transition zone separates the two layers. Fuis and others (1981) also suggest that a lower crustal structure consisting of diabase and gabbro is present beneath the metamorphosed sedimentary "basement".

The surface of the East Brawley KGRA consists of cultivated lacustrine deposits, except for the eastern edge which consists of sand dunes. Refraction seismic modeling by Fuis and others (1981) suggests that the unmetamorphosed sedimentary section extends to a depth of about 3 km in the eastern half of the East Brawley KGRA and deepens to about 4.3 km in the western half. The depth to the sub-basement correspondingly increases from about 12.3 km in the east to about 13.3 km in the west. The Wilson No. 1 well near the western boundary of the East Brawley KGRA penetrated sediments of the Colorado River delta to a total depth of 4,097 m (Muffler and White, 1969). Mineralogical changes observed in cuttings and core from the well indicate increasing diagenesis and thermal metamorphism with depth (Muffler and White, 1969). The appearance of substantial amounts of chlorite at about 1,800 m suggests the beginning of low-grade greenschist facies metamorphism.

PREVIOUS WELL DATA

The first indication of a deep, high-temperature hydrothermal system in the East Brawley - Glamis area occurred in 1963 when the Wilson No. 1 exploratory oil well encountered hot brines at a depth of approximately 4 km. The brine had a reported temperature of 260°C and a salinity of 54,000 ppm (Rex, 1971). In 1980 and early 1981, four geothermal exploration wells and one injection well were drilled to depths of 3 to 4 km. Locations of these wells are shown in Figure 9 and a brief description of each is given in Table 1. Little information is available on these wells, but scouting reports indicate that they are potentially producible.

Reed (1975) reports on the depths, temperatures, water chemistry and isotopic composition of produced waters for more than 30 thermal artesian wells in the East Brawley - Glamis area. Temperatures range from 30°C to 50°C with production depths ranging from 85 to 450 m. Bottom-hole temperatures increase approximately linearly with depth, consistent with a conductive gradient of about 87 °C km^{-1} (Figure 2). This gradient is compatible with the gradients of 60 to 95 °C km^{-1} calculated for the Wilson No. 1 well and the heat-flow boreholes (see Table 2). The concentrations of dissolved solids in waters produced from these wells range from 1,000 to 3,800 mg ℓ^{-1}, approximately an order of magnitude less than the deep brines encountered in the Wilson No. 1 well. This, along with the isotopic compositions, suggest that the near-surface (<500 m) waters are derived mainly from the Colorado River.

TABLE 1. Deep wells in the East Brawley KGRA

Well no. (Fig. 8)	Well name	Location (SBM)	Total depth (m)	Comments
1	East Highline 1	8-13S-16E	3,392	
2	Emanuelli 1	20-13S-16E		Drilling
3	Rutherford 1	19-13S-16E	3,271	
4	Borchard A-1	5-14S-16E	4,085	Producing interval 2,743 to 4,058 m
5	Borchard A-2	5-14S-16E	3,606	Injection well
6	Borchard A-3	8-14S-16E	3,928	Perforated liner at 3,532 to 3,906 m
7	Wilson 1	20-14S-15E	4,097	Abandoned oil and gas test well

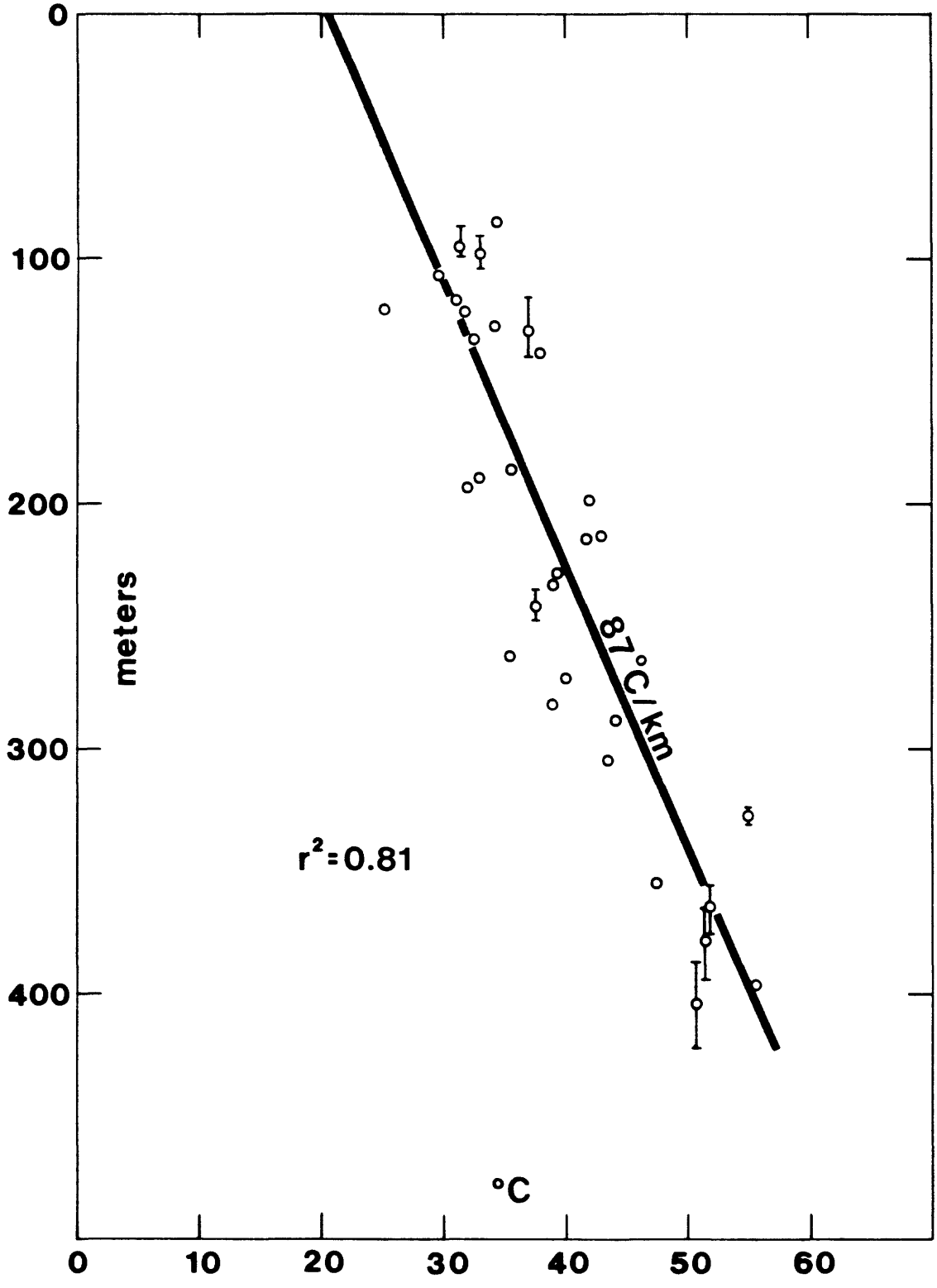

Figure 2. Temperature versus depth for 31 thermal artesian wells in the East Brawley - Glamis area. Vertical bars indicate production intervals. Temperature gradient determined by regression analysis. Well data from Reed (1975).

SUMMARY OF PREVIOUS GEOPHYSICAL INVESTIGATIONS

Bouger Anomaly Map

A complete Bouger anomaly map of the Salton Trough region is shown in Figure 3. The region exhibits a broad north-northwest positive Bouger anomaly coincident with the axis of the trough. Although underlain by 10 to 16 km of low density sediments (Fuis and others, 1981), the region is near sea level and is isostatically compensated suggesting marked crustal extension and thinning under the trough.

The broad positive high is punctuated with numerous "low-amplitude" local positive anomalies with closures of 2 to 20 mgals (∿2 mgals at Heber KGRA to 20+ mgals at the Salton Sea KGRA). The regions of gravity maxima, in every instance, coincide with regions of hydrothermal activity and high heat flow. The higher gravity near the heat-flow anomalies may reflect a combination of two processes: (1) the emplacement of rhyolitic and basaltic dikes and sills due to localized zones of rapid crustal extension occurring in the region of right-stepping offsets between active strands of right-lateral, strike-slip faults, and (2) the increased density of sediments due to cementation, recrystallization and thermal metamorphism by circulating hydrothermal fluids. Boreholes in the Salton Sea KGRA have encountered greenschist facies metamorphism, cementation of pore spaces and altered rhyolite and basalt dikes (Robinson and others, 1975). Browne (1977) reported on the occurrence and hydrothermal alteration of a diabase dike encountered in one of the wells drilled in the Heber KGRA. Based on the intense metamorphism of sediments observed within the Salton Sea KGRA,

Elders and others (1979) suggested that the more pervasive process and source of the excess mass is due to hydrothermal alteration of the sediments from rising plumes of hot brines. Active formation of greenschist facies rocks occurs within the Salton Sea field at depths of 1.0 to 2.5 km where temperatures range up to 365°C (Muffler and White, 1979; McDowell and Elders, 1979). Similar alteration and metamorphism is observed at Cerro Prieto (Elders and others, 1979), Heber (Browne, 1977), and East Mesa (Miller and Elders, 1980); however, the degree of recrystallization is less intense in these areas than at the Salton Sea field. In all of these fields, however, hydrothermal alteration has a pronounced effect on the physical properties of the sediments by reducing porosity and increasing density.

A local gravity maximum with approximately 5 mgals of closure (Figure 3) is contained within the boundaries of the East Brawley KGRA. The intimate association of hydrothermal systems with gravity maxima in the Salton Trough and the fact that the highest observed heat flow (Figure 9) coincides with the area of positive residual gravity strongly suggests the presence of a hydrothermal convective system beneath the East Brawley KGRA.

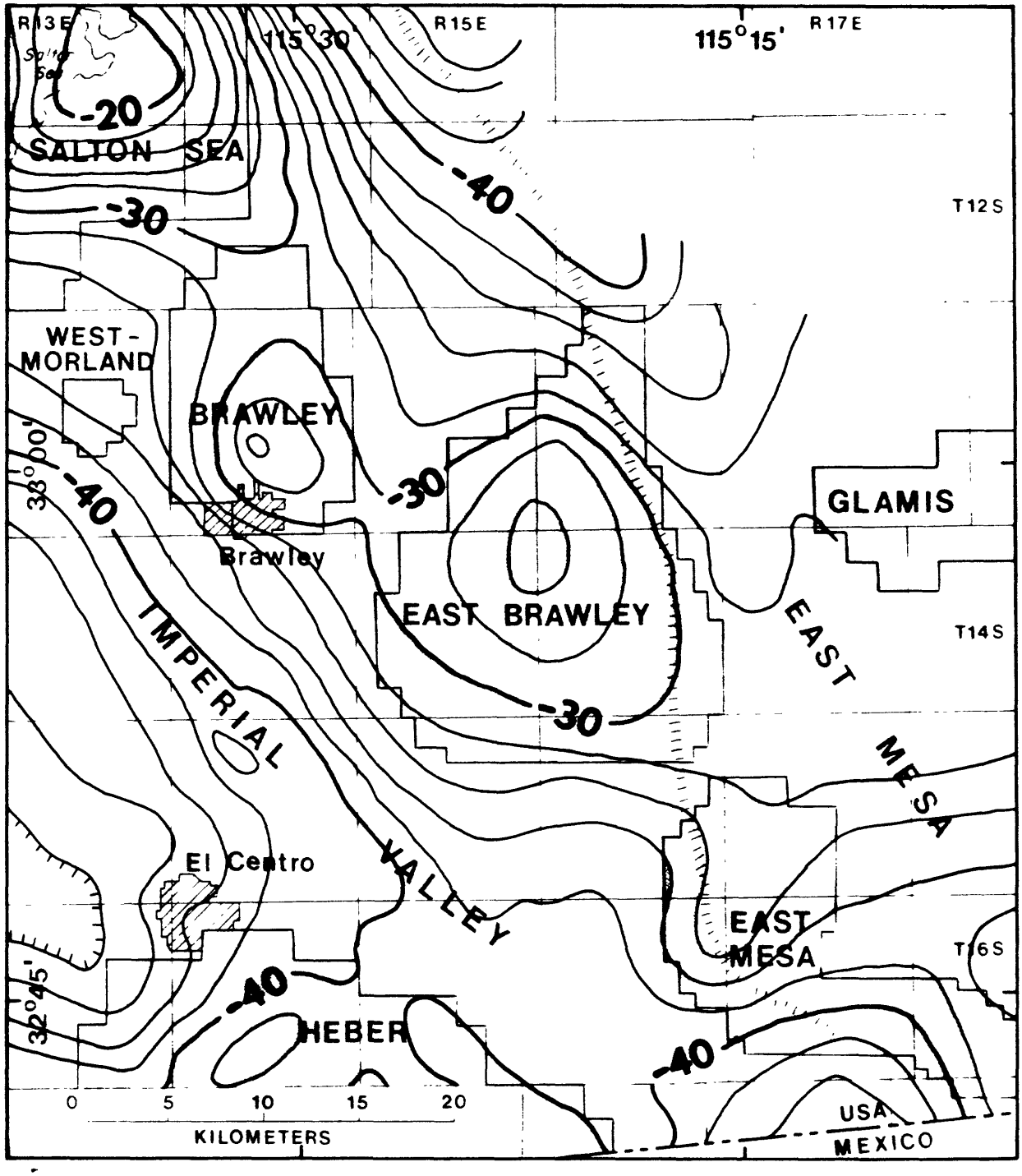

Figure 3. Complete Bouger gravity map of the Imperial Valley (modified from Biehler, 1971; Biehler and others, 1964). Contour interval, 2 mGals.

Electrical Resistivity

Inferences about the lateral extent of hydrothermal systems and the subsurface environment may be obtained from electrical resistivity. The resistivity of rocks in a given geothermal environment is due to two main conduction mechanisms. These mechanisms are electrolytic conduction through pore passages and fractures and surface conduction along mineral faces and clays. Therefore zones of low resistivity in a geothermal environment are probably caused by higher dissolved solid content of thermal waters as compared with groundwater, higher clay content due to hydrothermal alteration, increased fracture density and the high temperature of the thermal fluids. Electrical resistivity studies of the Imperial Valley have been conducted by Harthill (1978) and Meidav and Furgerson (1972). These studies indicate a general decrease in apparent resistivity within geothermal areas of the Salton Trough (i.e., Salton Sea, Brawley, Heber, and East Mesa fields). Figure 4 shows a lobe of low apparent resistivity (<3 ohm-m) extending into the East Brawley KGRA. This lobe coincides partly with the gravity (Figure 3) and heat-flow (Figure 9) maxima and can be interpreted as suggesting the presence of a hydrothermal system at depth.

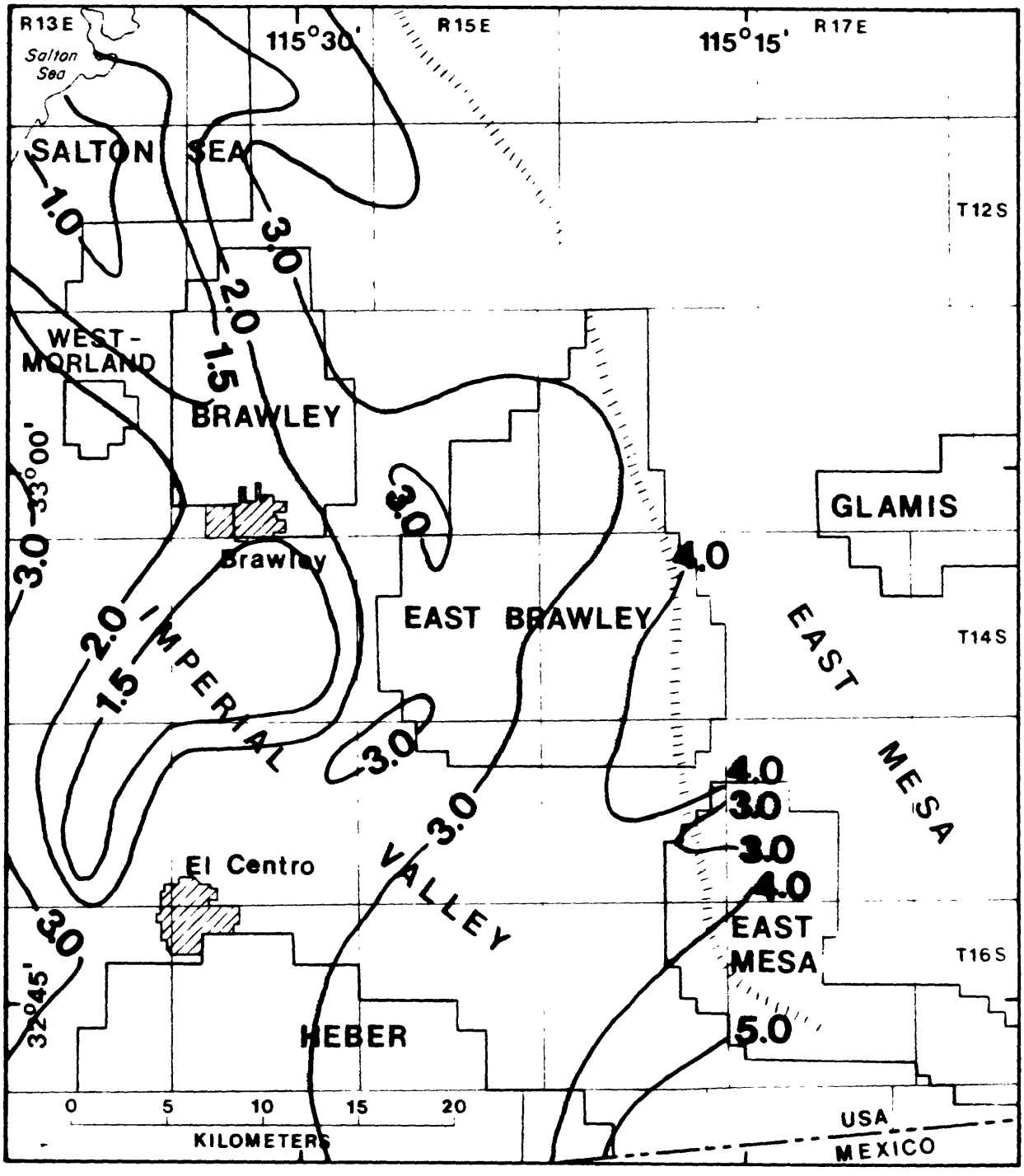

Figure 4. Map of apparent resistivity (in ohm-meters) of the Imperial Valley at a nominal penetration depth of 4 km (modified from Harthill, 1978).

HEAT-FLOW DATA

To provide background information for a geothermal resource assessment of the Glamis - East Brawley region, a series of 15 geothermal gradient - heat-flow boreholes was drilled. Real-time determinations of temperature, thermal conductivity, and hence, heat flow in these unconsolidated sediments were made in each hole using the downhole heat-flow probe illustrated schematically in Figure 5 and described in detail by Sass and others (1981). This method yields satisfactory determinations of both temperature gradient and thermal conductivity. Because formation temperatures are measured below the bit during the drilling operation, the hole need not be cased, and hence, can be backfilled immediately upon cessation of drilling. Since the thermal conductivities are measured in situ, we avoid the uncertainties that arise in determining a formation conductivity for unconsolidated sediments from estimates of formation porosity and the solid component conductivity (usually determined from chip samples, which are subject to a substantial loss of the fine-grained fraction, see discussion in Appendix II).

Figure 6 illustrates temperature-depth points determined from downhole probe runs in uncased holes. Except for GL09, these holes show approximately the same linearly extrapolated surface temperature (~28°C) which is to be expected for closely spaced boreholes drilled in a flat terrain where the dominant mode of heat transfer is by conduction. We found it necessary to case seven of the 15 boreholes for one or both of the following reasons: (1) the invasion of drilling fluids around the probe during the temperature run, and (2) inconsistencies between successive runs caused by

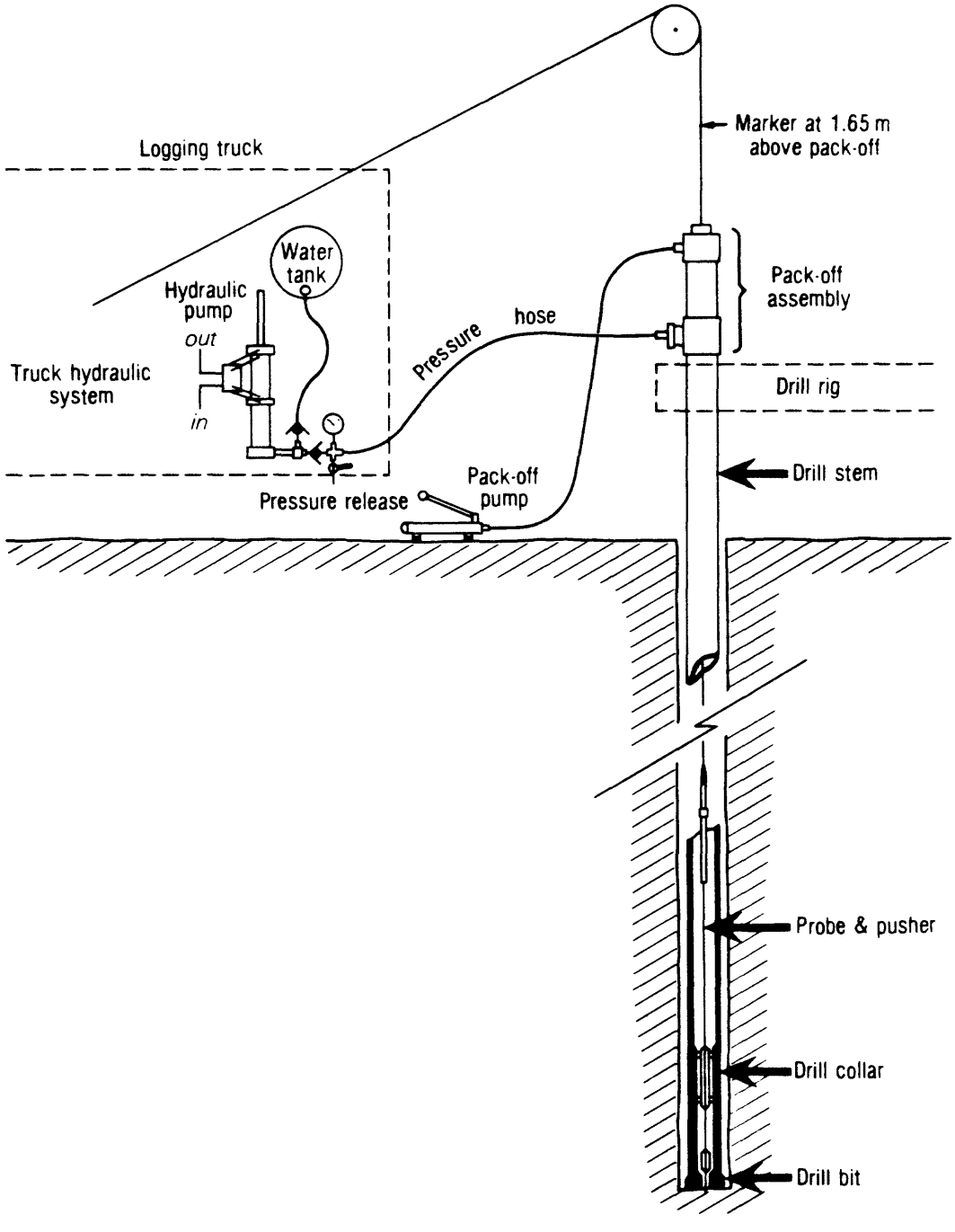

Figure 5. Schematic diagram of field setup for downhole probe experiment (from Sass and others, 1981).

vertical water movement in the formation. Temperature-depth points determined from probe runs in the seven cased holes are shown in Figure 7. Our primary criterion for running casing in the wells during this study should be apparent from a comparison of Figures 6 and 7. The tendency for the gradient to change significantly between successive probe runs and the wide scatter exhibited in extrapolated surface temperatures in the wells illustrated in Figure 7 strongly suggest a vertical component of downward water movement, making any estimates of conductive heat flows based on successive probe runs meaningless; therefore, the holes were cased so that a detailed determination of the temperature-depth profile could be made. The most recent temperature-depth profiles for the seven cased holes are shown in Figure 8 (individual temperature profiles are shown in Appendix I). The upper segments of the profiles from GL08, GL16, GL25, GL27, and GL28 are undulant, suggesting a combination of upward, downward, and lateral movement of groundwater. Since these boreholes are located within areas of intensely irrigated farmland, their undulant character is consistent with the slow downward percolation of surface irrigation waters into near-surface lacustrine sediments. Below the zone of water infiltration, the profiles yield consistent gradients suggesting that heat transfer in the lower segments is primarily by conduction. GL19 is located 50 m to the east of the Coachella Canal; in this instance, the strong undulant nature exhibited by the temperature-depth profile can be explained by a combination of downward and lateral water seepage from the canal into the surrounding porous, fine-grained arkosic sands.

The non-linearity of the temperature profiles as discussed above and shown in Figure 8 indicates that a substantial part of the near-surface (<100 m) heat flow beneath cultivated areas is non-conductive. The low

thermal gradient and undulant character in the upper part of the profiles from these areas strongly suggest that heat from a greater depth is being absorbed by surface infiltration of irrigation waters into near-surface strata. Therefore, boreholes of depths less than 100 m will not yield an accurate representation of the heat flow at depth in cultivated areas where irrigation is intense.

Downhole probe runs, cased hole temperatures, and heat-flow calculations are summarized for the 15 new holes in Table 2. (For details on the calculation of temperatures and in situ thermal conductivities from downhole probe runs, see Sass and others, 1981.) The vertical component of heat flow, q, for successive downhole probe runs was computed as the product of the harmonic mean thermal conductivity, $\langle K_f \rangle$, determined in situ, and the temperature gradient, Γ, determined for successive runs. For cased holes, q was computed for linear segments of the temperature profile as the product of the least-squares temperature gradient and the harmonic thermal conductivity, $\langle K_f \rangle$. The locations of the boreholes along with contoured heat flow for the region are illustrated in Figure 9.

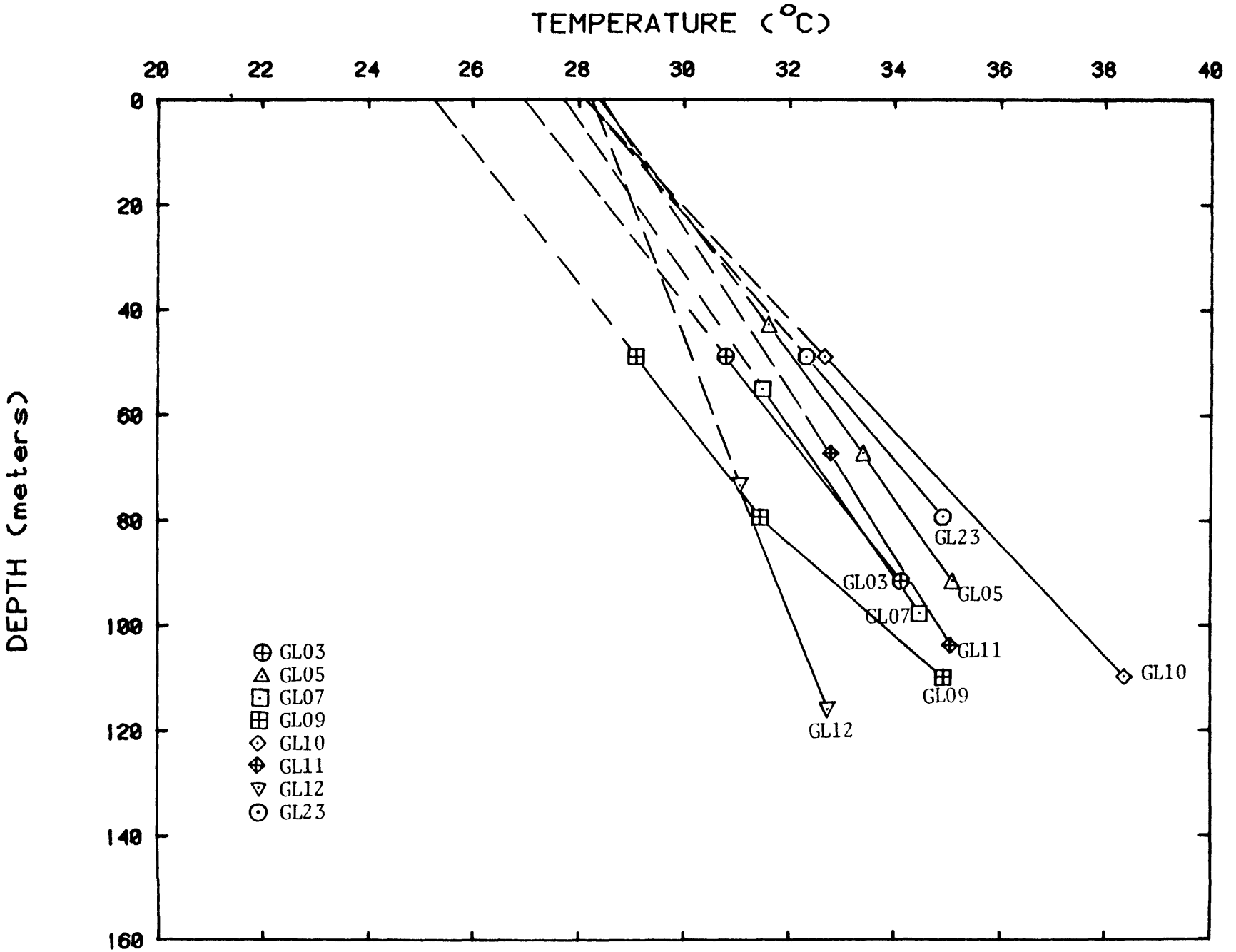

Figure 6. Temperature-depth points determined from downhole probe runs in uncased holes.

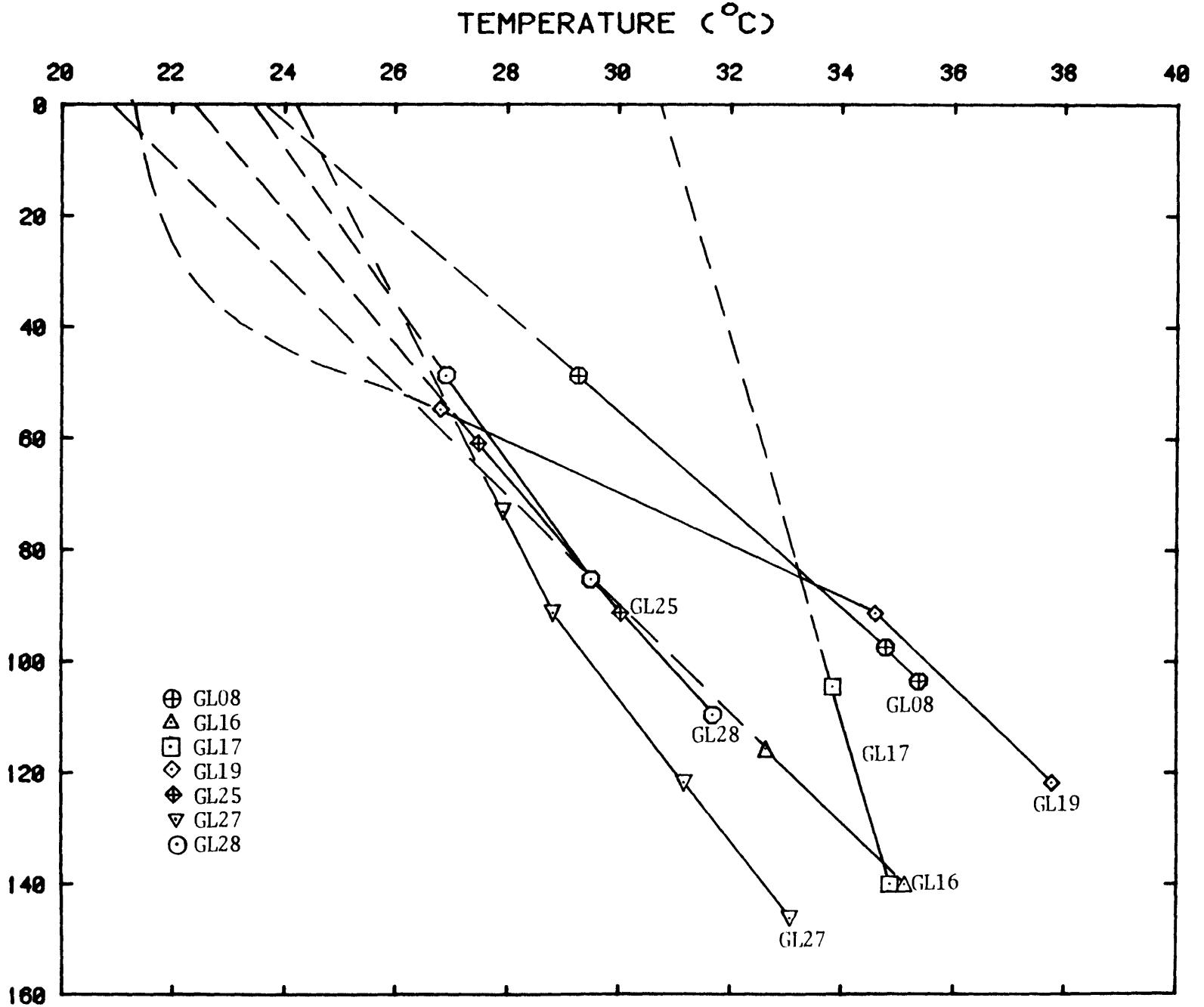

Figure 7. Temperature-depth points determined from downhole probe runs in holes that were cased upon completion.

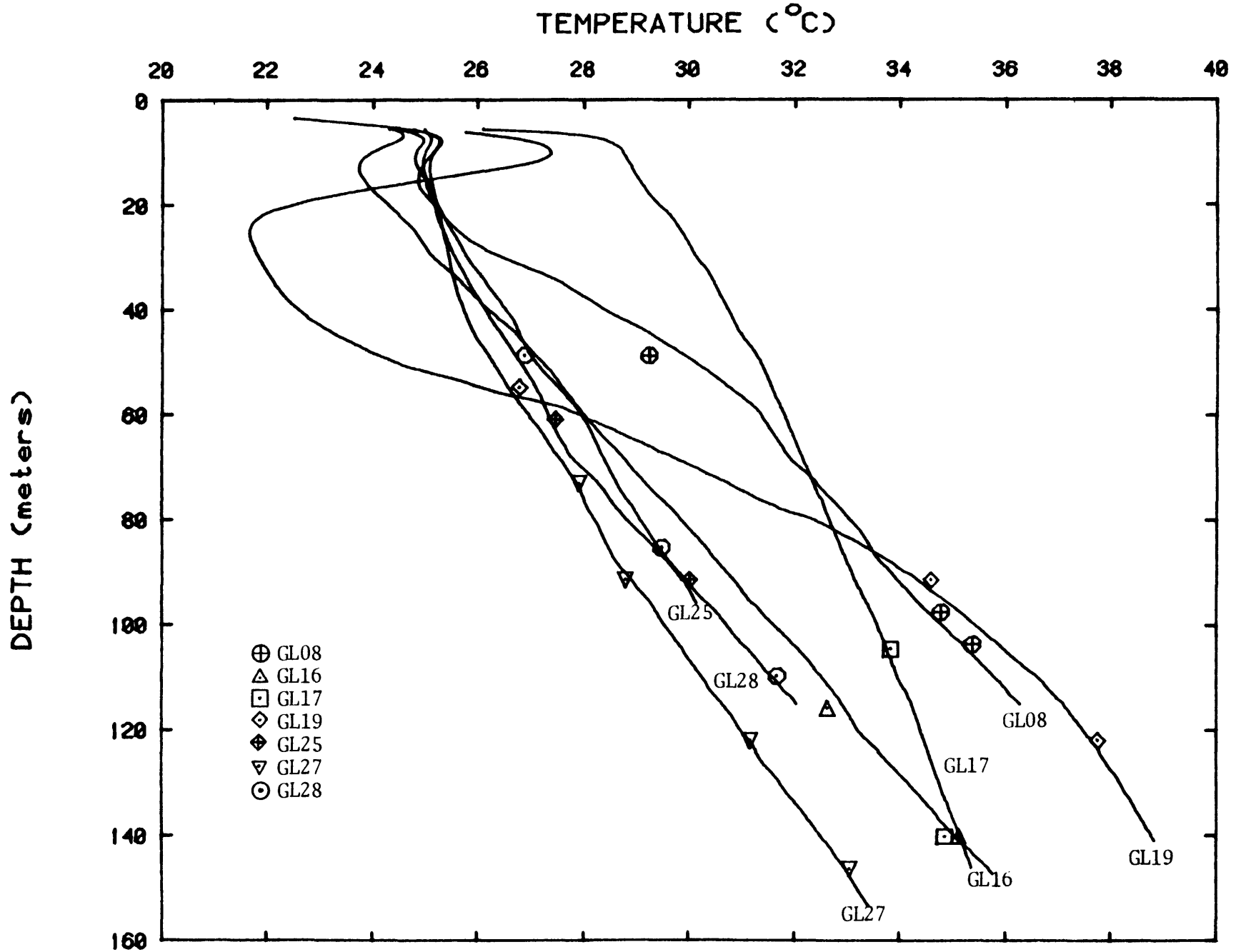

Figure 8. Temperature profiles from cased USGS wells in the East Brawley - Glamis area. Individual temperature-depth points from downhole probe runs are shown as symbols.

TABLE 2. Heat-flow summary for Glamis and East Brawley KGRA's

Well Designation	Lat.	Long.	Depth Run (ft)	(m)	θ(°C)	Q-probe K(W m^{-1} °K^{-1})	Q-probe Γ(°K km^{-1})	Q-probe q(mWm^{-2})	Depth interval (m)	Cased hole Temperature logs Γ(°K km^{-1})	Cased hole Temperature logs q(mW m^{-2})	Final q(mWm^{-2})
GL03	32° 57.1'	115° 15.2'	160 300	48.77 91.44	30.78 34.13	1.65 (.08) ¶	78(4)	129(19)	†	†	†	129
GL05	33° 00.2'	115° 15.1'	140 220 300	42.67 67.06 91.44	(31.59) 33.40 35.10	¶ 1.87 (.03) 1.69 (.17)	70(4)	127(20)	†	†	†	127
GL07	33° 02.4'	115° 15.9'	180 320	54.86 97.54	31.48 34.48	1.63 (.01) 1.64 (.04)	70(5)	115(20)	†	†	†	115
GL08*	33° 05.2'	115° 18.4'	160 320 340	48.77 97.54 103.63	29.27 34.80 35.39	1.59 (.01) ¶ 1.53 (.15)	113(4) 97(8) 111(4)	174(8)	60-115	90(4)	141(8)	141
GL09	33° 04.4'	115° 20.7'	160 260 360	48.77 79.25 109.73	29.08 (31.44) 34.93	1.52 (.05) ¶ 1.58 (.02)	96(3)	149(20)	†	†	†	149
GL10	33° 00.9'	115° 06.0'	160 360	48.77 109.73	32.65 38.37	1.38 (.18) 2.45 (.13)	94(3)	166(51)	66-87	98**(6)	173(59)	166
GL11	33° 02.6'	115° 03.4'	220 340	67.06 103.63	32.77 35.06	2.28 (.20) 2.42 (.03)	63(5)	148(16)	58-98	65**(4)	153(14)	148
GL12	33° 04.6'	115° 11.5'	240 380	73.15 115.82	31.06 32.72	2.05 (.01) 2.42 (.03)	39(4)	87(18)	†	†	†	87
GL16*	32° 54.9'	115° 21.7'	380 460	115.82 140.21	32.64 35.14	¶ ¶	103(8)	237(49)	44-147	86(7)	198(42)	198
GL17	32° 53.3'	115° 06.8'	343 460	104.55 140.21	33.85 (34.88)	2.45 (.25) ¶	29(5)	71(19)	50-154	42(5)	103(23)	103
GL19*	32° 58.4'	115° 11.0'	180 300 400	54.86 91.44 121.92	26.80 34.61 37.77	1.76 (.25) ¶ ¶	***	***	***	***	***	***
GL23	33° 07.7'	115° 19.4'	160 260	48.77 79.25	32.30 34.92	2.49 (.03) 1.62 (.05)	86(6)	160(29) ††	†	†	†	160††
GL25*	32° 53.4'	115° 24.3'	200 300	60.96 91.44	27.48 30.04	2.04 (.13) 2.64 (.15)	84(3)	193(32)	68-96	89(4)	205(36)	205
GL27*	33° 04.4'	115° 24.8'	240 300 400 480	73.15 91.44 121.92 146.30	27.92 28.82 31.18 33.07	2.07 (.34) ¶ 1.91 (.07) 2.09 (.04)	46 77 66 77 77 70(3)	141(11)	86-154	73(2)	147(9)	147
GL28*	33° 00.5'	115° 24.6'	160 280 360	48.77 85.34 109.73	26.90 29.51 31.69	1.76 (.18) ¶ 1.65 (.07)	72(10) 89(16) 79(3)	134(9)	80-115	88(6)	150(15)	150

*Cased holes.
**Gradients measured open hole.
***Gradient and heat flow have not been estimated for boreholes exhibiting easily identifiable hydrologic disturbances.
†Uncased holes.
††Heat flow corrected for a two-layered conductivity medium.
¶Conductivity determinations invalid due to invasion of drilling fluid.

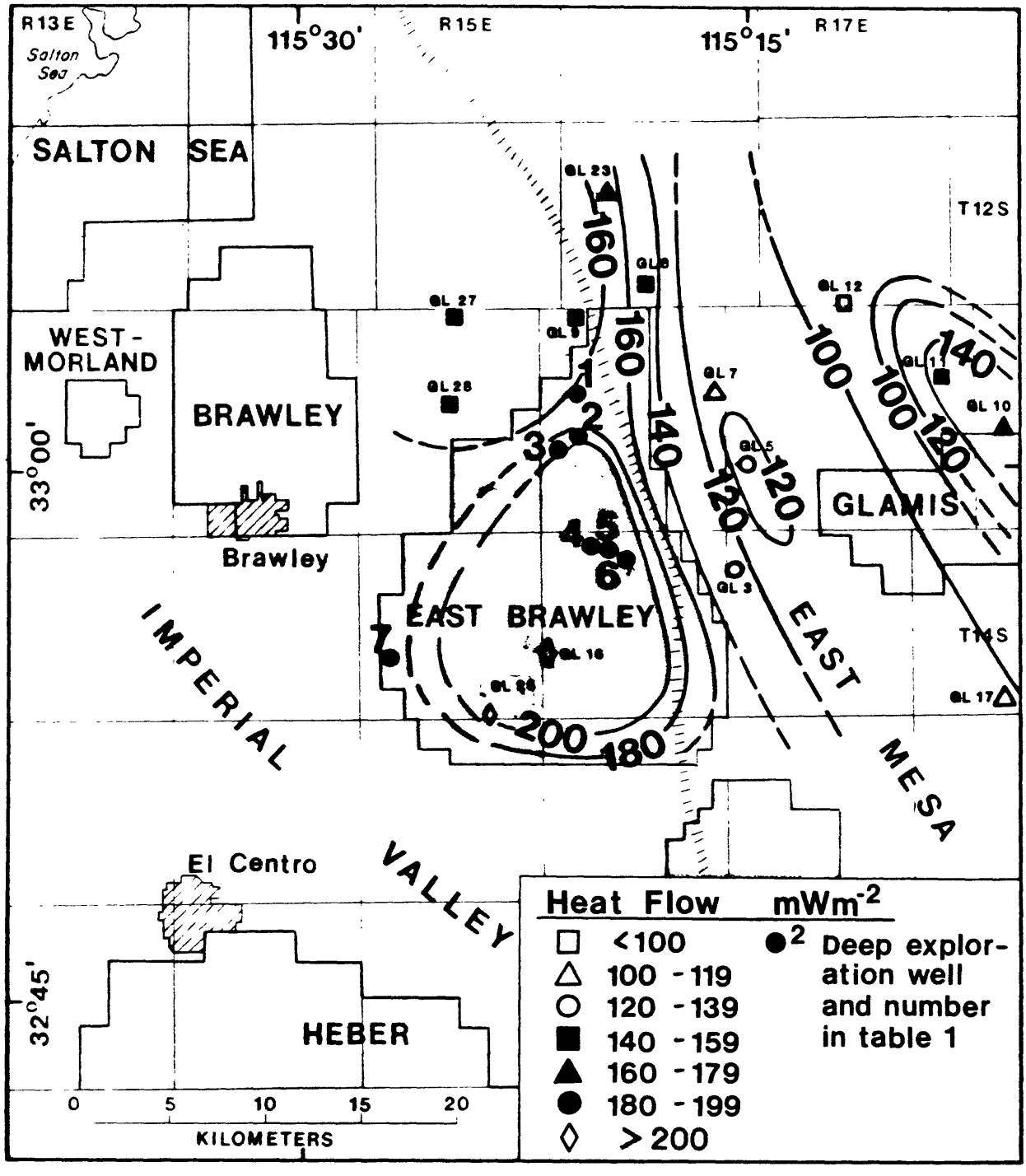

Figure 9. Heat flow of the East Brawley - Glamis area showing locations of heat-flow boreholes and deep exploration wells. Contour interval 20 mWm^{-2}.

DISCUSSION

Regional heat flow in the Salton Trough is anomalously high (>100 mWm^{-2}, Sass and others, 1981; Combs, 1971) and locally quite variable. Evidence for distributed tectonic extension and magmatic activity throughout the Salton Trough imply that much of the anomalous heat-flow results from the vertical mass flow into the lithosphere from the asthenosphere required to accommodate the extension (see e.g., Lachenbruch and Sass, 1978). In a similar way, rapid local extension, in which diverging mass is replaced by rising basalt, can account for the high heat flow observed locally at volcanic centers within the trough (e.g., Salton Sea, Cerro Prieto). Such centers probably occur in the region of right-stepping offsets between active strands of right-lateral, strike-slip faults where the local extensional rate may exceed the regional rate by an order of magnitude.

The heat-flow data for the Glamis - East Brawley region shown in Figure 9 indicate that the central portion of the Salton Trough has heat flow in excess of 140 mWm^{-2} and that the eastern periphery of the trough may be marked by a rapid transition to a heat flow typical of the Basin and Range ($\sim$80 mWm^{-2}). The local heat-flow anomalies shown for East Brawley and Glamis KGRA's (Figure 9) are poorly controlled and somewhat speculative. In both cases, we have two high heat-flow values with limited spatial control, but in spite of this we have drawn in heat-flow contours based on the strong correlation of heat-flow and gravity maxima observed for the Salton Trough. Both the gravity and heat flow imply the convective transfer of large amounts of heat at depth which is consistent with rapid local extension, magmatic intrusion and hydrothermal convection at depth resulting from a "leaky" transform fault; however, there is no seismic evidence for a spreading center beneath either of these areas.

REFERENCES

Biehler, Shawn, 1971, Gravity studies in the Imperial Valley, in Rex, R. W., (PI), Cooperative geological-geophysical-geochemical investigations of geothermal resources in the Imperial Valley area of California: University of California, Riverside, p. 29-41.

Biehler, Shawn, Kovach, R. L., and Allen, C. R., 1964, Geophysical framework of the northern end of the Gulf of California structural province, in van Andel, T. H., and Shor, G. G., Jr., eds., Marine geology of the Gulf of California: American Association of Petroleum Geologists Memoir 3, p. 126-143.

Browne, P. R. L., 1977, Occurrence and hydrothermal alteration of diabase Heber geothermal field, Imperial Valley, California: University of California, Riverside, Institute of Geophysics and Planetary Physics Report 77/9.

Combs, J., 1971, Heat flow and geothermal resource estimates for the Imperial Valley, in Rex, R. W., (PI), Cooperative geological-geophysical-geochemical investigations of geothermal resources in the Imperial Valley area of California: University of California, Riverside, p. 5-28.

Elders, W. A., Rex, R. W., Meidav, T., Robison, P. T., and Biehler, Shawn, 1972, Crustal spreading in southern California: Science, v. 178, p. 15-24.

Elders, W. A., Hoagland, J. R., McDowell, S. D., and Cobo, J. M., 1979, Hydrothermal mineral zones in the geothermal reservoir of Cerro Prieto, in Elders, W. A., ed., Geology and geothermics of the Salton Trough (Guidebook: Field Trip no. 7, prepared by Geological Society of America Bulletin, 92nd annual conference): University of California, Riverside, Campus Museum Contributions, no. 5, p. 36-43.

Fuis, G. S., Mooney, W. D., Healy, J. H., McMechan, G. A., and Lutter, W. S., 1981, Crustal structure of the Imperial Valley region: U.S. Geological Survey Professional Paper, in press.

Harthill, Norman, 1978, A quadripole resistivity survey of the Imperial Valley, California: Geophysics, v. 43, p. 1485-1500.

Lachenbruch, A. H., and Sass, J. H., 1978, Models of an extending lithosphere and heat flow in the Basin and Range province: Geological Society of America Memoir 152, p. 209-250.

McDowell, S. D., and Elders, W. A., 1979, Geothermal metamorphism of sandstone in the Salton Sea geothermal system, in Elders, W. A., ed., Geology and geothermics of the Salton Trough (Guidebook: Field Trip no. 7, prepared by Geological Society of America Bulletin, 92nd annual conference): University of California, Riverside, Campus Museum Contributions, no. 5, p. 70-76.

Meidav, Tsvi, and Furgerson, R., 1972, Resistivity studies of the Imperial Valley geothermal area, California: Geothermics, v. 1, p. 47-62.

Miller, K. R., and Elders, W. A., 1980, Geology, hydrothermal petrology, stable isotope geochemistry, and fluid inclusion geothermometry of LASL geothermal test well C/T-1 (Mesa 31-1), East Mesa, Imperial Valley, California, USA: Los Alamos Scientific Laboratory, Report LA-8515-MS, 61 p.

Muffler, L. J. P., and White, D. E., 1969, Active metamorphism of upper Cenozoic sediments in the Salton Sea geothermal field and the Salton Trough, southeastern California: Geological Society of America Bulletin, v. 80, p. 157-182.

Reed, M. J., 1975, Chemistry of thermal water in selected geothermal areas of California: California Division of Oil and Gas Report No. TR 15, 31 p.

Robinson, P. T., Elders, W. A., and Muffler, L. J. P., 1976, Quaternary volcanism in the Salton Sea geothermal field, Imperial Valley, California: Geological Society of America Bulletin, v. 87, p. 347-360.

Sass, J. H., Blackwell, D. D., Chapman, D. S., Costain, J. K., Decker, E. R., Lawver, L. A., and Swanberg, C. A., 1981, Heat flow from the crust of the United States, in Touloukian, Y. S., Judd, W. R., and Roy, R. F., eds., Physical Properties of Rocks and Minerals: McGraw-Hill Book Company, p. 503-548.

Sass, J. H., Kennelly, J. P., Jr., Wendt, W. E., Moses, T. H., Jr., and Ziagos, J. P., 1981, In-situ determination of heat flow in unconsolidated sediments: Geophysics, v. 46, p. 76-83.

APPENDIX I

TEMPERATURE MEASUREMENTS

Temperature measurements were made in boreholes of 90 to 150 m depths drilled using conventional mud rotary techniques. Well completion involved lowering 33 mm I.D. steel pipe to within a meter of bottom, then pumping about 0.7 m^3 of cement-bentonite grout through the pipe, followed by a wiping plug and clear water (for detailed description, see Moses and Sass, 1979). This amount of grout is usually sufficient to seal off the lowermost 50 m of the annulus around the pipe in these 130 mm nominal diameter holes. An additional ∿3 m of cement plug was emplaced at the top of the well after the remainder of the hole had been backfilled with mud and cuttings. Upon completion of the well, the steel pipe was then filled with water and allowed to equilibrate to facilitate temperature measurements (better heat transfer between probe and surrounding rock). Chip samples for thermal conductivity measurements were collected at 6-m intervals in all holes.

Temperatures were measured repeatedly to a few millidegrees at intervals of .3 m until all transient disturbances resulting from drilling had vanished. Temperature profiles are presented graphically in Figures I-1 through I-7. A smoothed average gradient over 6-m intervals is also shown on each of these figures. Individual temperatures determined from the lowermost thermistor for each probe run are plotted as open circles on the diagrams. The temperatures obtained during drilling generally are in agreement with the later ones (with some systematic offsets probably related to differences in reference levels); however, there are some substantial disagreements in some wells (see e.g., Figures I-1 and I2). These disagreements reflect mostly artesian water flows in the annulus between casing and borehole wall. Temperatures in the grouted sections of the wells generally are coherent and

where a disagreement exists (e.g., Figure I-3) it reflects an invasion of drilling fluids around the probe during the temperature run.

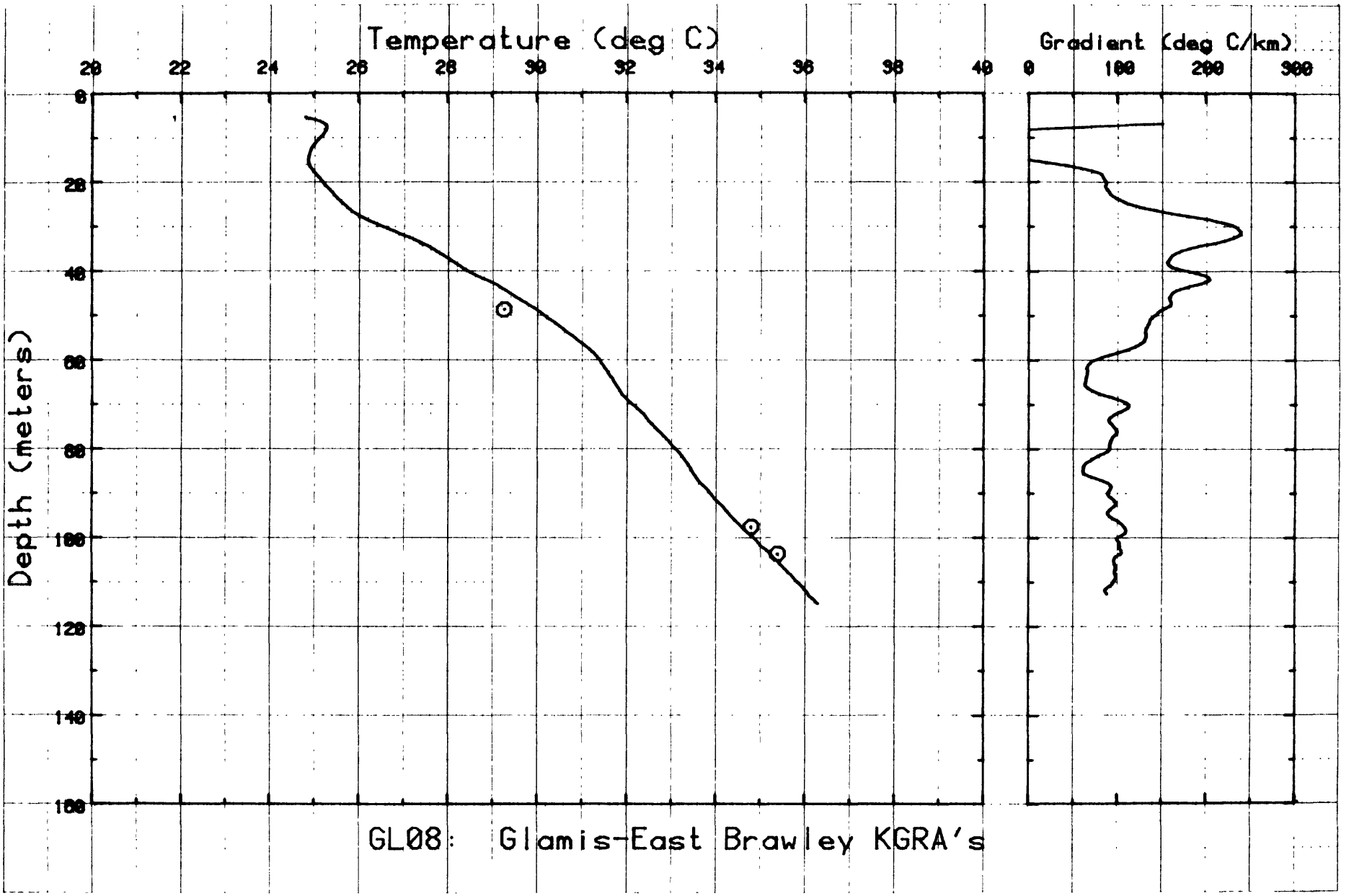

Figure I-1. Temperature and gradients for borehole GL08.

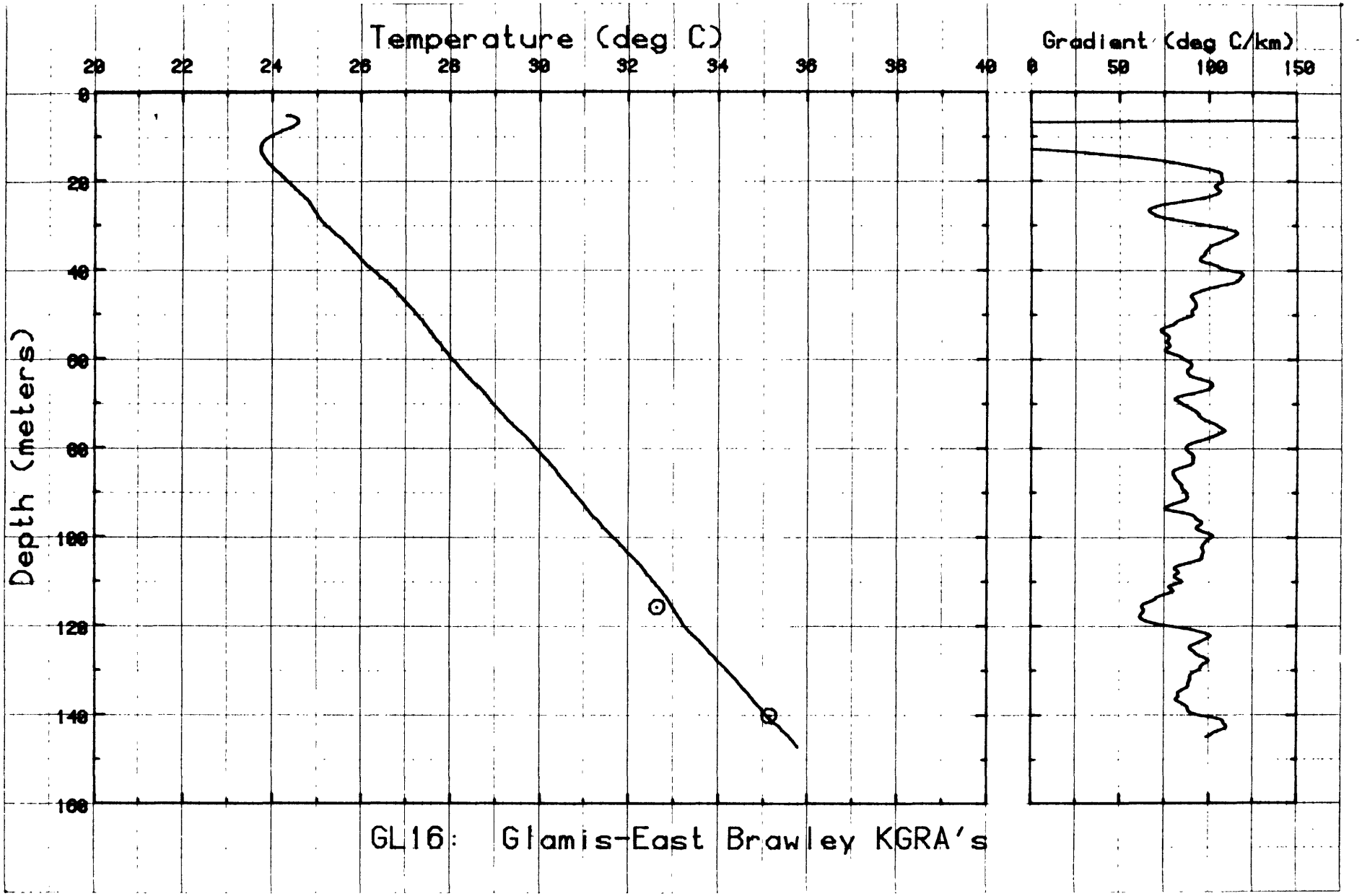

Figure I-2. Temperature and gradients for borehole GL16.

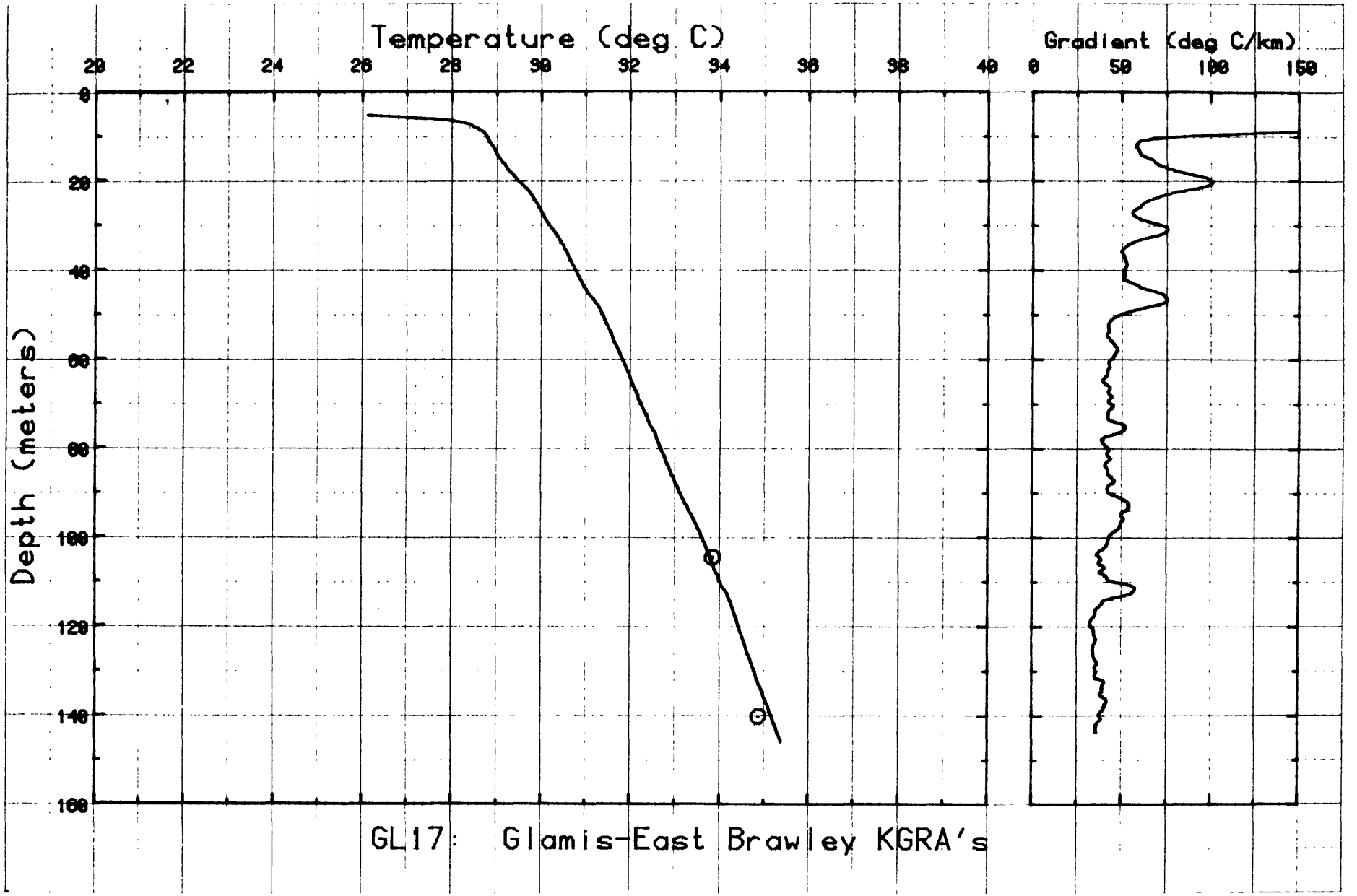

Figure I-3. Temperature and gradients for borehole GL17.

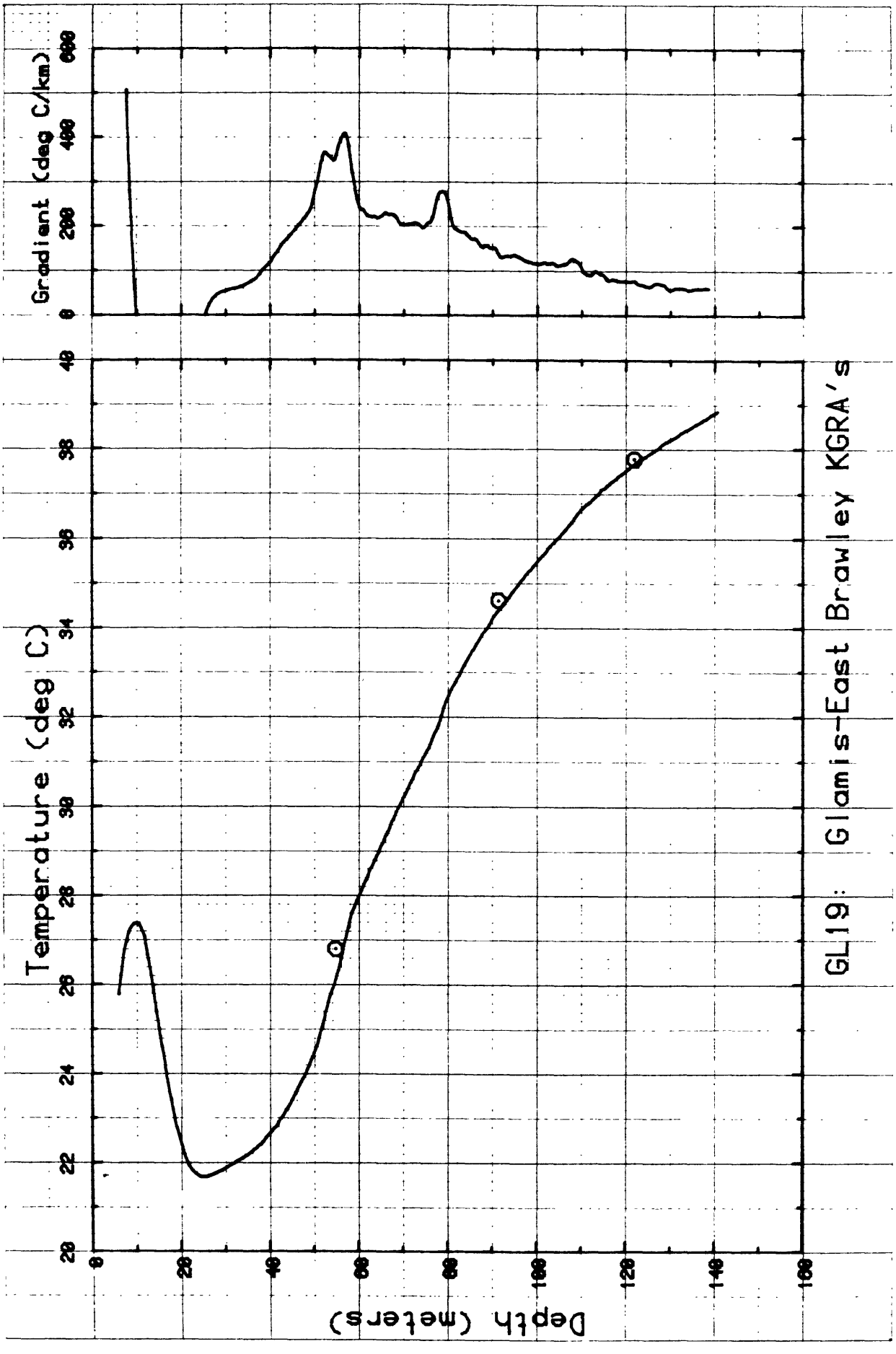

Figure I-4. Temperature and gradients for borehole GL19.

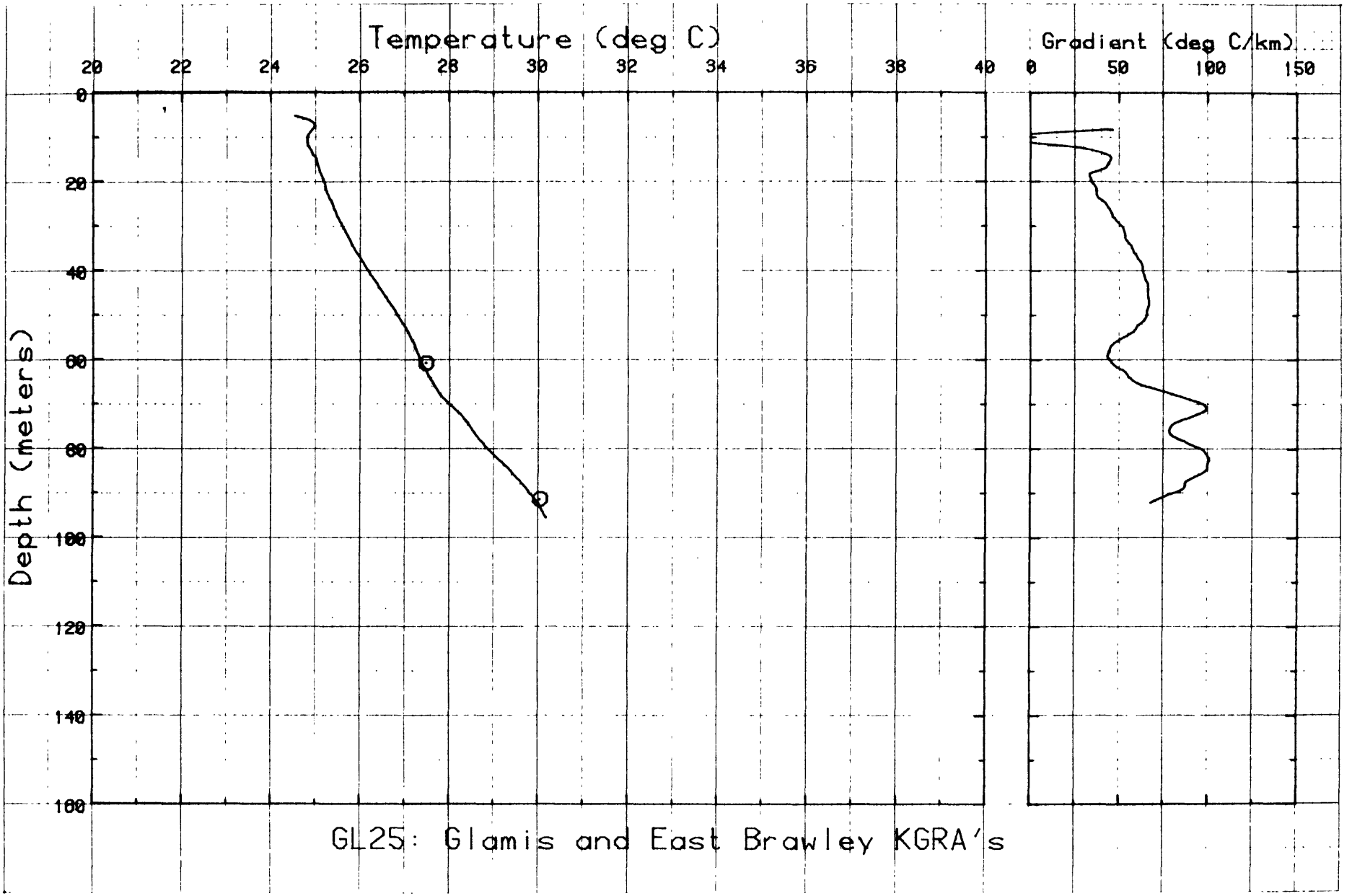

Figure I-5. Temperature and gradients for borehole GL25.

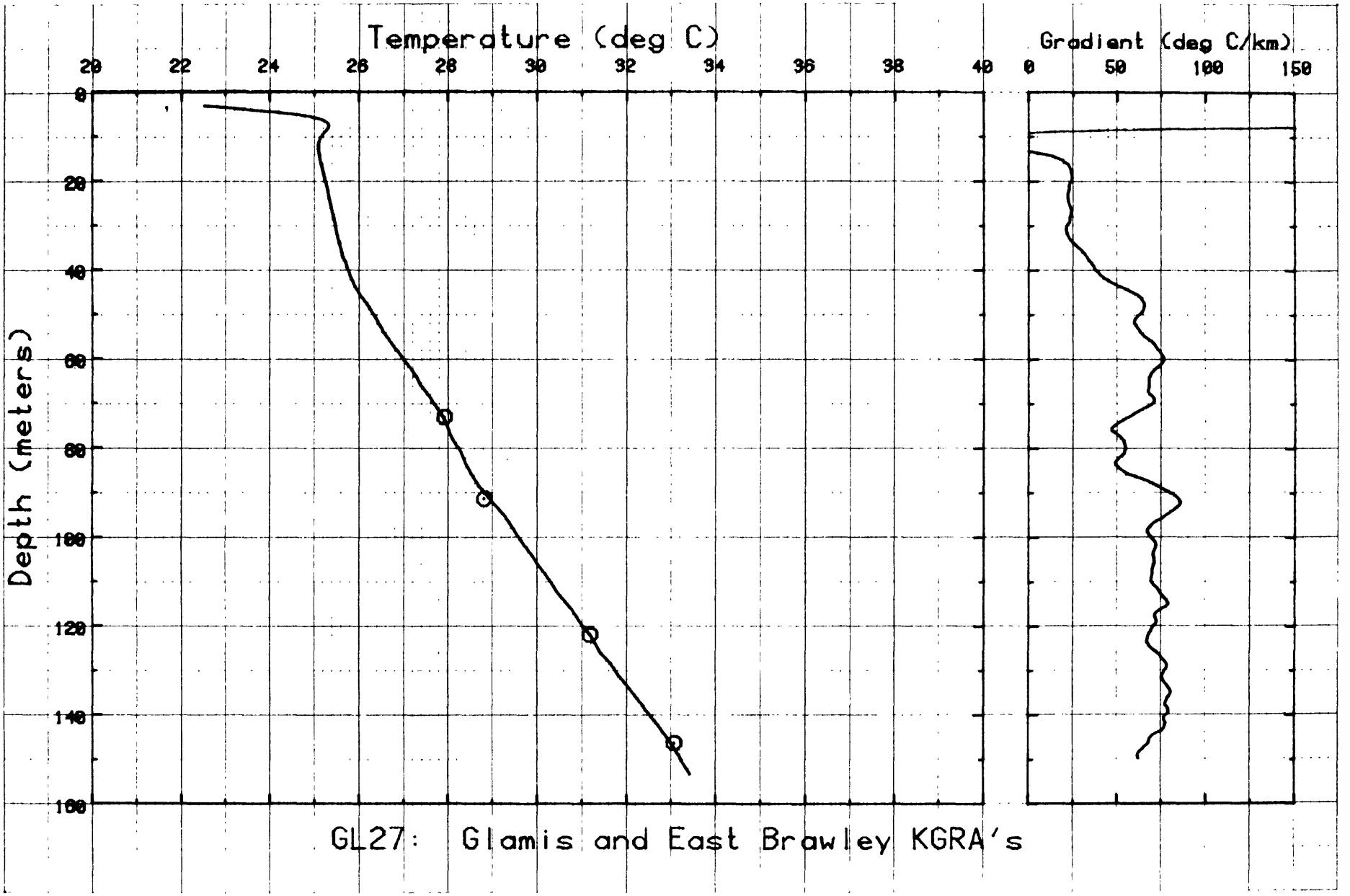

Figure I-6. Temperature and gradients for borehole GL27.

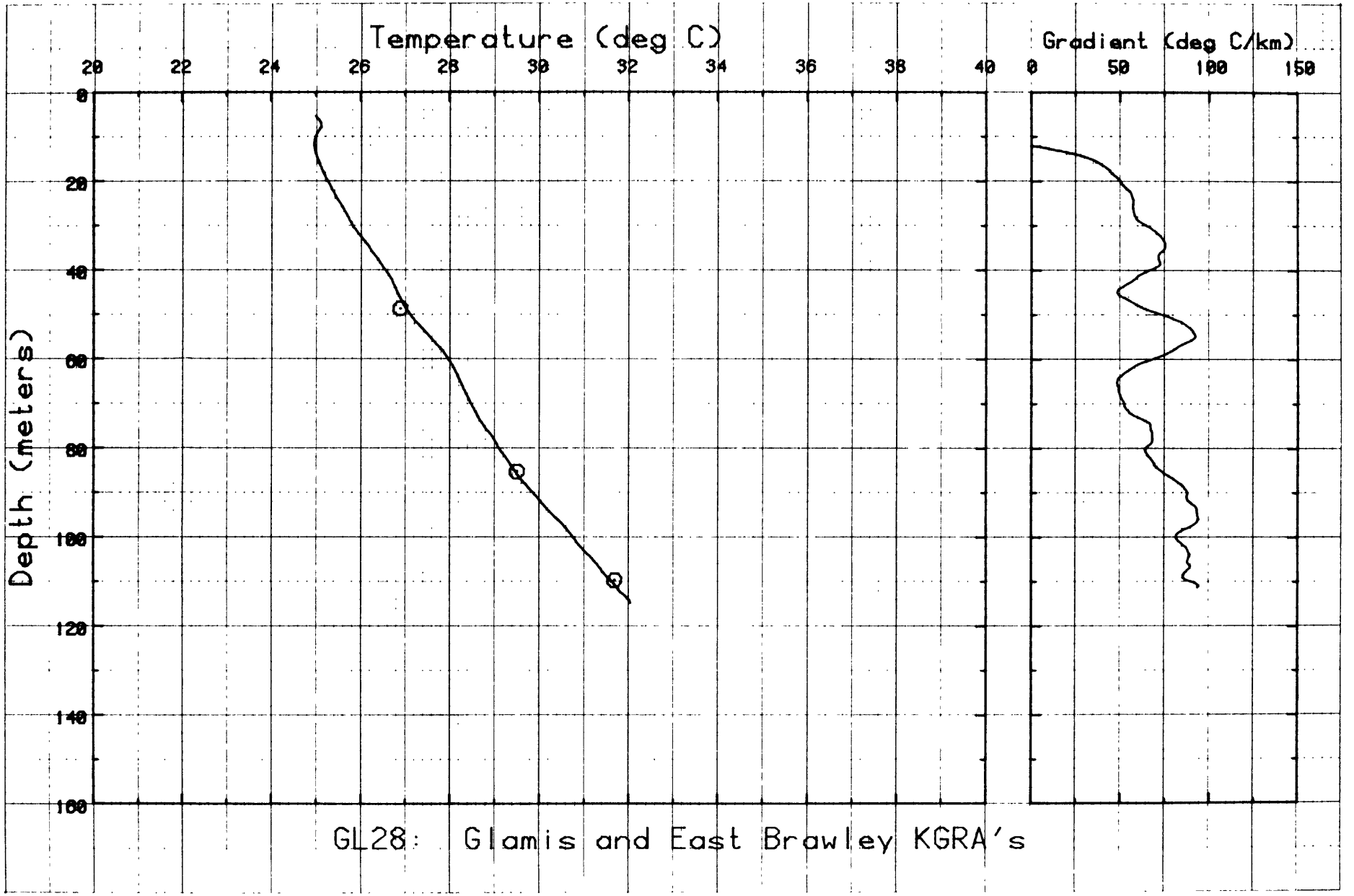

Figure I-7. Temperature and gradients for borehole GL28.

APPENDIX II

THERMAL CONDUCTIVITIES

Two types of thermal conductivity measurement were performed. Where a successful penetration of the formation by the downhole probe was achieved and when there was no evidence of downward invasion by drilling fluid of the formation being tested, we were able to obtain a reliable value of thermal conductivity using the in situ method as described by Sass and others (1981). For the first two holes (GL09 and GL27), no samples of cuttings were collected. Samples from three other holes (GL05, GL07, and GL08) were lost. Conductivities of the solid components of samples from the remaining holes were determined using the chip technique described by Sass and others (1971).

Conductivity values vary widely (Table II-1 and Figure II-1) with means of 1.87 ± 0.05 $Wm^{-1} K^{-1}$ for in situ determinations and 3.03 ± 0.08 for the solid component based on measurements of drill cuttings.

In very permeable sands, the formation was often invaded by drilling fluids. This was quite obvious in the passive temperature record following insertion of the probe and no values are shown for these instances in Table II-1. Thus we have great confidence in the in situ conductivity values (K_f) that we have tabulated and where the solid component conductivities (K_s) are lower than the in situ values (as at 91 m in GL25), the latter values are suspect. That is not to say that the measurements are incorrect; we suspect rather, that the sampling procedure in this instance was selective and that we lost a substantial fraction of the high conductivity fines.

We calculated values of the porosity (ϕ) by combining K_s and K_f using a geometric mean model and also noted a great deal of scatter (Table II-1). The overall mean of $26 \pm 3\%$ for the interpreted porosity is, however, quite reasonable for this poorly sorted sedimentary material.

As an exercise, we calculated heat flows in a conventional manner, using chip conductivities and our derived value of porosity. There are some rather large discrepancies between downhole probe heat flows and those calculated conventionally. This did not alarm us inasmuch as all holes that were cased constitute "problem wells" and showed evidence for hydrologic disturbances during the real time downhole probe runs. A comparison of the conductivity columns does, however, demonstrate the kinds of errors we might expect in conductivity using chip conductivities and a generalized value of porosity.

Table II-1. Summary of thermal conductivities, Glamis - East Brawley KGRA's
(Standard errors in parentheses; standard deviations in brackets)

Hole	Depth (ft)	Depth (m)	K_s* ($Wm^{-1}\,°K^{-1}$)	Q-probe Depth (ft)	Q-probe Depth (m)	K_f** ($Wm^{-1}\,°K^{-1}$)	$\phi^{\dagger}$ (%)
GL03	75	22.9	3.99				
	115	35.0	4.78				
	155	47.2	1.88	160	48.8	1.65 (.08)	11 (5)
	185	56.4	2.08				
	235	71.6	2.79				
	275	83.8	3.39				
	295	89.9	2.92	300	91.4	------	
	315	96.0	2.38				
			$\bar{K}_s$ = 2.77 (.30) [.86]			$\bar{K}_f$ = 1.65 (.08)	$\bar{\phi}$ = 34 (7)
GL10	95	29.0	3.34				
	135	41.1	3.16				
	155	47.2	3.36	160	48.8	1.38 (.18)	51 (11)
	175	53.3	3.09				
	215	65.5	3.59				
	255	77.7	3.32				
	295	89.9	3.53				
	335	102.1	3.64				
	355	108.2	3.48	360	38.4	2.45 (.13)	20 (4)
	375	114.3	3.79				
			$\bar{K}_s$ = 3.42 (.07) [.22]			$\bar{K}_f$ = 1.77 (.49) [.70]	$\bar{\phi}$ = 38 (16)
GL11	75	22.9	3.48				
	115	35.0	3.19				
	155	47.2	3.04				
	195	59.4	3.48				
	215	65.5	3.29	220	67.1	2.28 (20)	21 (6)
	235	71.6	3.46				
	275	83.8	3.64				
	315	96.0	3.43				
	335	102.1	3.21	340	103.6	2.42 (.03)	18 (3)
	355	108.2	3.10				
			$\bar{K}_s$ = 3.33 (.06) [.18]			$\bar{K}_f$ = 2.35 (.07) [.10]	$\bar{\phi}$ = 20 (2)
GL12	75	22.9	3.18				
	115	35.0	3.17				
	155	47.2	3.19				
	195	59.4	3.14				
	235	71.6	3.32	240	73.2	2.05 (.01)	28 (4)
	275	83.8	3.12				
	315	96.0	3.02				
	355	108.2	3.53				

Table II-1. Summary of thermal conductivities, Glamis - East Brawley KGRA's (continued)
(Standard errors in parentheses; standard deviations in brackets)

Hole	Depth (ft)	Depth (m)	K_s* ($Wm^{-1}\,°K^{-1}$)	Q-probe Depth (ft)	Q-probe Depth (m)	K_f** ($Wm^{-1}\,°K^{-1}$)	ϕ† (%)
GL12	375	114.3	3.10	380	115.8	2.41 (.04)	15 (3)
	395	120.4	3.85				
			$\bar{K}_s$ = 3.25 (.07) [.23]			$\bar{K}_f$ = 2.22 (.18) [.25]	$\bar{\phi}$ = 22 (5)
GL16	95	29.0	3.03				
	135	41.1	2.33				
	175	53.3	2.33				
	215	65.5	2.53				
	225	77.7	2.52				
	355	108.2	2.26	380	115.8	------	---
	415	126.5	2.19				
	455	138.7	2.10	460	140.2	------	---
			$\bar{K}_s$ = 2.38 (.09) [.26]				
GL17	75	22.9	2.82				
	115	35.0	3.40				
	155	47.2	3.27				
	195	59.4	3.49				
	235	71.6	4.69				
	275	83.8	5.02				
	315	96.0	5.10				
	335	102.1	2.69	343	104.6	2.45 (.25)	6 (7)
	355	108.2	4.75				
	395	120.4	3.00				
	435	132.6	4.02				
	455	138.7	2.90	460	140.2	------	---
	475	144.8	3.68				
			$\bar{K}_s$ = 3.58 (.22) [.79]			$\bar{K}_f$ = 2.45 (.25)	$\bar{\phi}$ = 21 (6)
GL19	135	41.1	4.56				
	175	53.3	3.42	180	54.9	1.76 (.25)	38 (10)
	215	65.5	4.50				
	255	77.7	4.84	300	91.4	------	---
	375	114.3	5.10				
	415	126.5	5.02	400	121.9	------	---
	455	138.7	4.79				
			$\bar{K}_s$ = 4.53 (.26) [.68]			$\bar{K}_f$ = 1.76 (.25)	$\bar{\phi}$ = 46 (8)
GL23	75	22.9	3.48				
	115	35.0	2.47				

Table II-1. Summary of thermal conductivities, Glamis - East Brawley KGRA's (continued)
(Standard errors in parentheses; standard deviations in brackets)

Hole	Depth (ft)	Depth (m)	K_s* ($Wm^{-1}\,°K^{-1}$)	Q-probe Depth (ft)	Q-probe Depth (m)	K_f** ($Wm^{-1}\,°K^{-1}$)	$\phi^{\dagger}$ (%)
GL23	155	47.2	3.94	160	48.8	2.49 (.03)	24 (4)
	195	59.4	4.27				
	235	71.6	3.41				
	255	77.7	2.34	260	79.3	1.62 (.05)	27 (5)
	275	83.8	2.42				
			$\bar{K}_s$ = 3.03 (.28) [.75]			$\bar{K}_f$ = 1.96 (.42) [.59]	$\bar{\phi}$ = 27 (14)
GL25	95	29.0	1.97				
	135	41.1	2.14				
	175	53.3	2.20				
	195	59.4	2.64	200	61.0	2.04 (.13)	17 (10)
	215	65.5	3.49				
	255	77.7	2.66				
	295	89.9	2.54	300	91.4	2.64 (.15)	-3 (5)
	315	96.0	2.25				
			$\bar{K}_s$ = 2.42 (.14) [.40]			$\bar{K}_f$ = 2.30 (.30) [.42]	$\bar{\phi}$ = 4 (13)
GL28	95	29.0	2.17				
	135	41.1	2.28				
	155	47.2	2.81	160	48.8	1.76 (.18)	30 (8)
	175	53.3	2.38				
	215	65.5	2.99				
	255	77.7	2.75				
	275	83.8	2.88	280	85.3	------	
	295	89.9	2.16				
	335	102.1	2.30				
	355	108.2	2.49	360	109.7	1.65 (.07)	29 (6)
	375	114.3	2.72				
			$\bar{K}_s$ = 2.47 (.09) [.29]			$\bar{K}_f$ = 1.70 (.05) [.08]	$\bar{\phi}$ = 26 (3)

*K_s, solid component conductivity measured from chips.

**K_f, in situ formation conductivity measured with Q-probe.

$^{\dagger}\phi$, porosity deduced from thermal conductivity measurements, $\phi = \ell n(K_f/K_s)/\ell n(K_w/K_s)$.

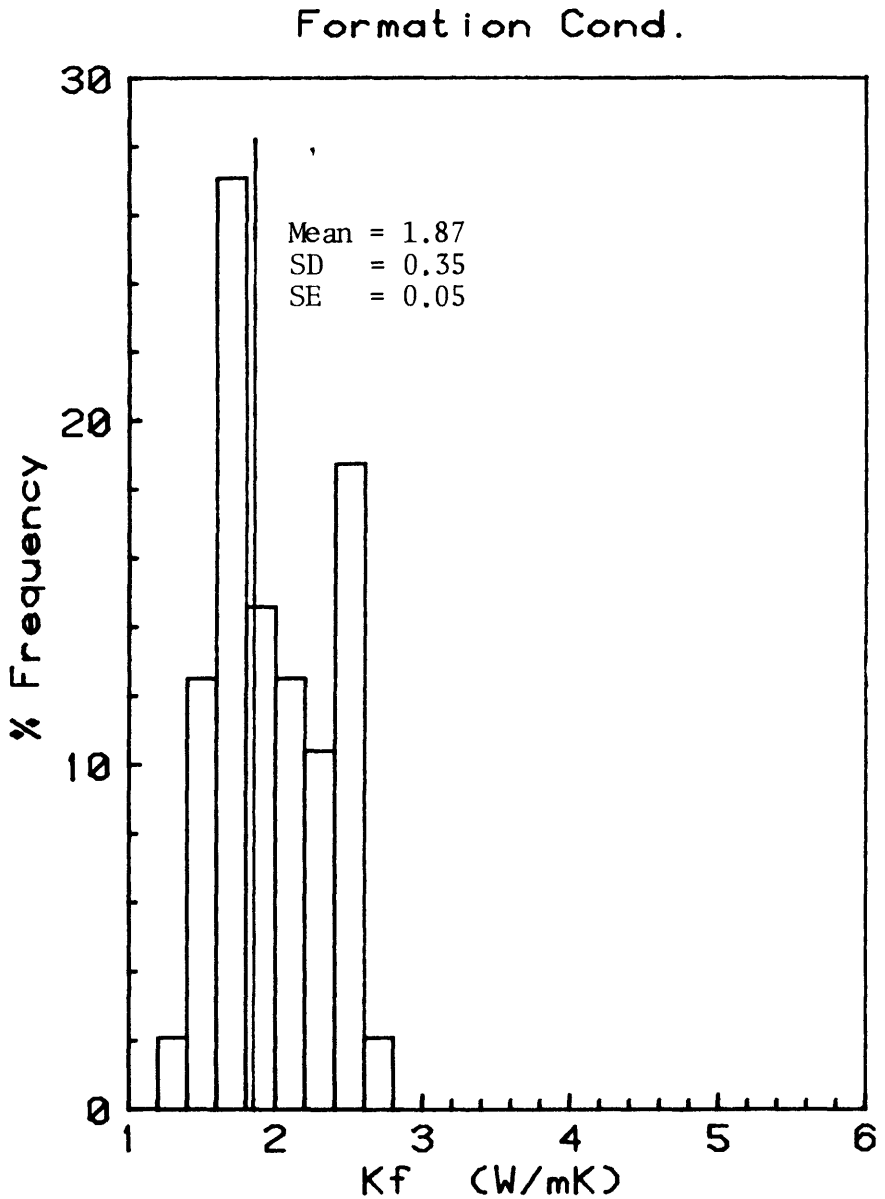

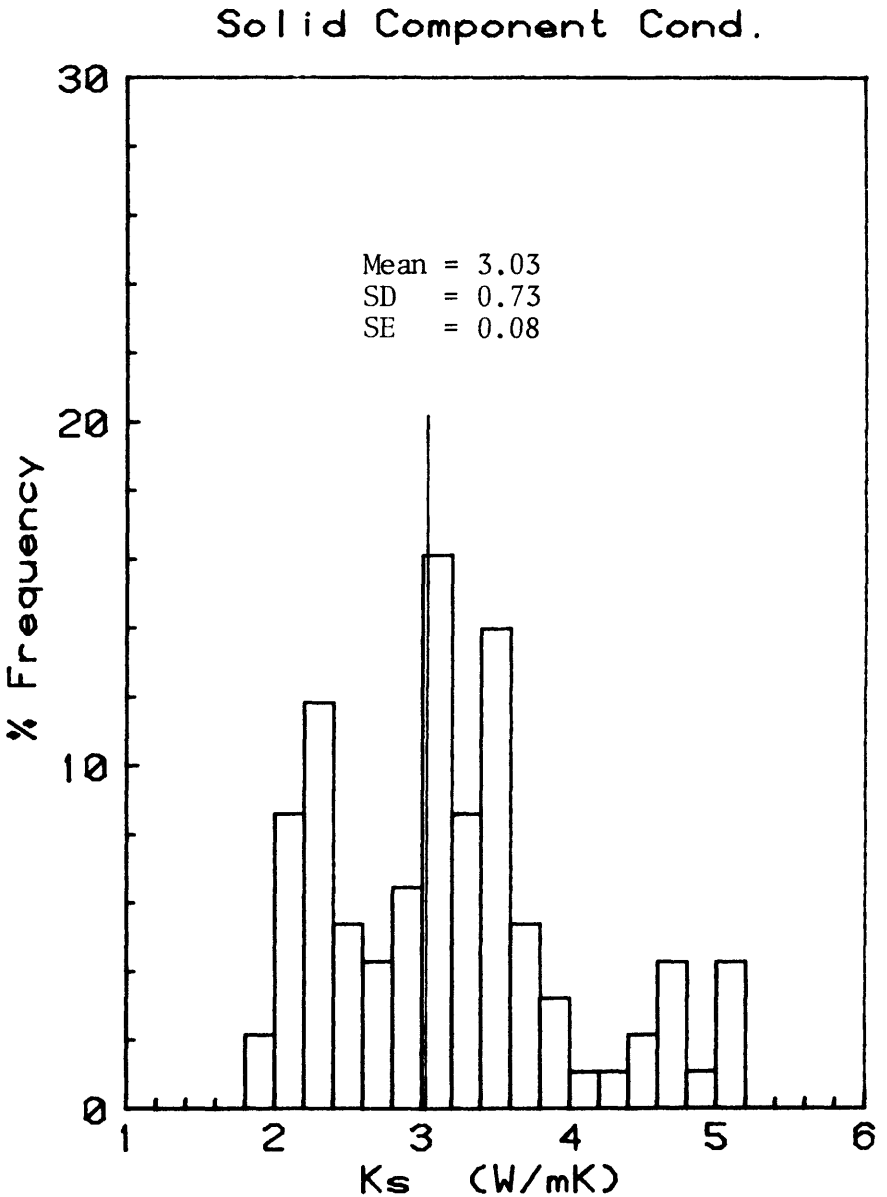

Figure II-1. Histograms illustrating the distribution of thermal conductivity for both in situ determinations of formation conductivity (K_f) and laboratory determinations of the conductivity of drill cuttings (K_s).

TABLE II-2. Comparison of interval heat flow determined between downhole probe runs and heat flow determined from the cased hole temperature log and chip conductivities

		Q-probe			Cased hole temperature log			
	Depth interval (m)	Γ (°K km^{-1})	K_f (Wm^{-1} °K^{-1})	q (mWm^{-2})	Γ (°K km^{-1})	$\bar{K}_s$ (Wm^{-1} °K^{-1})	$\bar{K}_f$ (Wm^{-1} °K^{-1})†	q (mWm^{-2})
GL08	48.8-103.6	111 (4)	1.57 (.02)	174 (8)	89 (4)	**	**	**
	48.8- 97.5	113 (4)	1.59 (.01)	180 (7)	89 (4)	**	**	**
	97.5-103.6	97 (8)	1.53 (.15)	148 (27)	107 (8)	**	**	**
GL10	48.8-109.7	94 (3)	1.77 (.49)	166 (51)	98* (6)	3.46 (.08)	2.18 (.47)	214* (59)
GL11	67.1-103.6	63 (5)	2.35 (.07)	148 (16)	63* (4)	3.35 (.08)	2.13 (.45)	134* (37)
GL16	115.8-140.2	103 (8)	***	***	89 (5)	2.18 (.05)	1.55 (.24)	138 (29)
GL17	104.6-140.2	29 (5)	2.45 (.25)	71 (19)	38 (4)	3.37 (.29)	2.14 (.47)	81 (26)
GL19	54.9-121.9	63 (3)	***	***	166 (19)	4.53 (.30)	2.67 (.67)	443 (162)
	54.9- 91.4	213 (10)	1.76 (.25)	375 (71)	219 (15)	4.16 (.46)	2.50 (.62)	548 (173)
	91.4-121.9	104 (5)	***	***	109 (8)	4.97 (.09)	2.86 (.73)	312 (102)
GL25	70.0- 91.4	84 (3)	2.30 (.30)	193 (32)	87 (3)	2.66 (.18)	1.80 (.34)	157 (35)
GL27	73.1-146.3	70 (3)	2.02 (.07)	141 (11)	72 (2)	**	**	**
	73.1-121.9	66 (4)	1.98 (.10)	131 (15)	70 (3)	**	**	**
	91.4-146.3	77 (4)	2.00 (.06)	154 (13)	73 (2)	**	**	**
	73.1- 91.4	46 (4)	2.07 (.24)	95 (19)	55 (4)	**	**	**
	91.4-121.9	77 (6)	1.91 (.05)	147 (15)	72 (2)	**	**	**
	121.9-146.3	77 (6)	1.00 (.06)	154 (7)	77 (4)	**	**	**
GL28	48.8-109.7	79 (3)	1.70 (.05)	134 (9)	71 (4)	2.53 (.10)	1.73 (.31)	123 (29)
	48.8- 85.3	72 (10)	1.76 (.18)	127 (31)	63 (8)	2.75 (.11)	1.84 (.34)	116 (36)
	85.3-109.7	89 (16)	1.65 (.08)	147 (34)	88 (5)	2.30 (.07)	1.61 (.27)	142 (32)

†Formation conductivities have been calculated for $\bar{\phi}_f$ = 26% ± 12% S.D.
*Gradients measured open hole.
**No drill cuttings available for measurement of $\bar{K}_s$.
***Conductivity results invalid due to invasion of drilling fluids.

APPENDIX III

OPEN-HOLE LOGS

Open-hole logs consisting of caliper, self-potential, pole-dipole resistivity and gamma ray were obtained for each borehole, with the exceptions of GL03 and GL07 where hole caving prevented their running, and are illustrated in Figures III-1 through III-13. The recordings were made with analog equipment and then digitized at 0.3 m intervals for playback at different scales. In general, for sedimentary sections consisting primarily of Holocene deltaic and lacustrine deposits a small resistivity along with a large increase in the gamma ray and self-potential represents a clayey section of the formation. For cased holes the average temperature-gradient over 1-m intervals is shown for comparison with the open-hole logs. For sedimentary sections with constant heat flux across the section changes in the temperature-gradient logs are inversely proportional to changes in the formation thermal conductivity which, in unconsolidated sediments, primarily reflect a change in the sand-shale ratio of the formation. For example, as the formation becomes more clayey, the thermal conductivity decreases, causing an increase in the temperature gradient. Qualitatively, temperature gradients correlate best with gamma-ray logs with both exhibiting a pronounced increase in clayey sections of the boreholes. Less pronounced correlations are noted with the resistivity and self-potential and may be attributed to the fact that both the sandy and clayey sections are saturated with saline waters, thereby making it difficult to distinguish between the sections on the basis of resistivity.

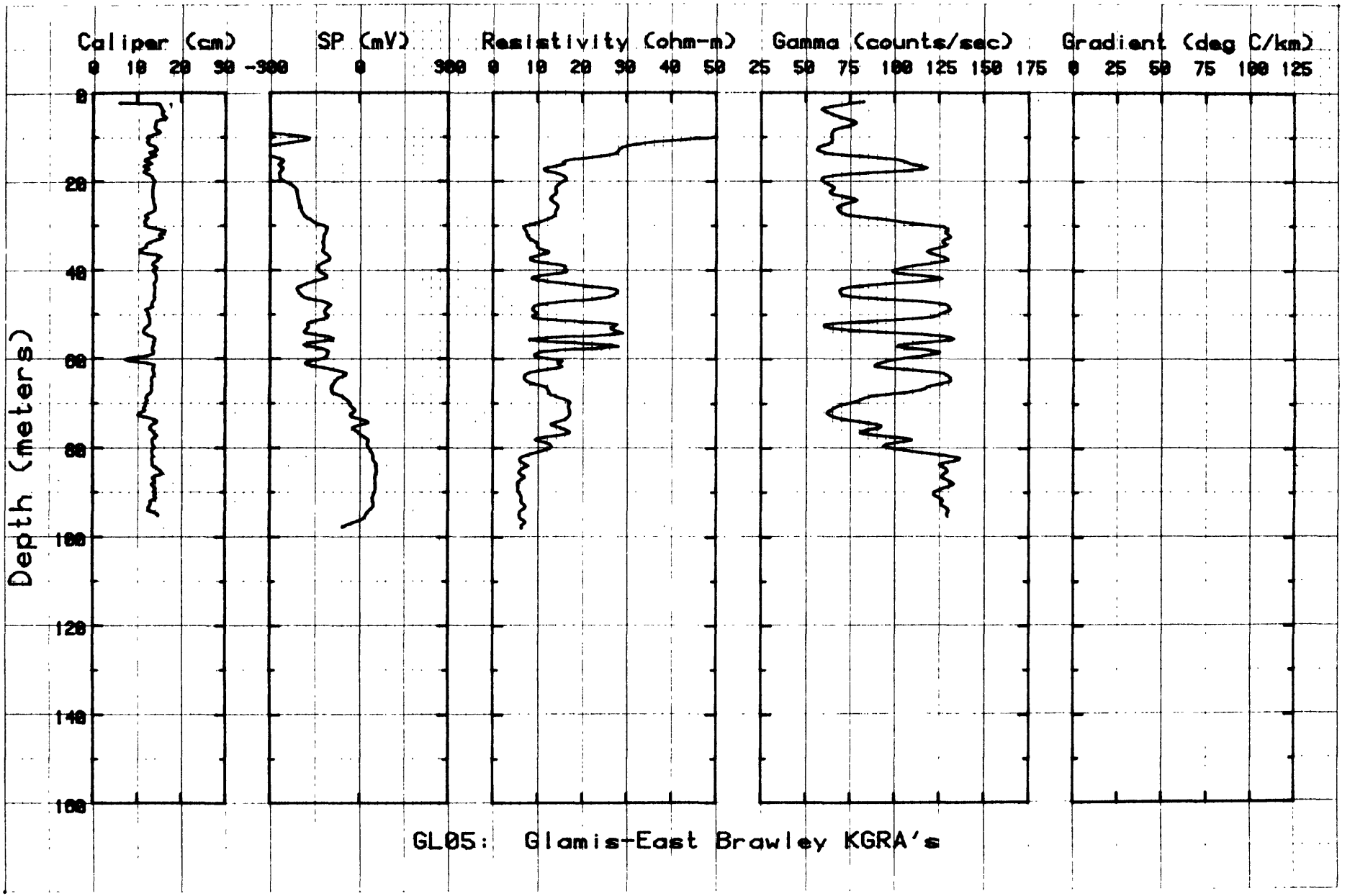

Figure III-1. Caliper, self-potential, resistivity, and gamma-ray logs for borehole GL05.

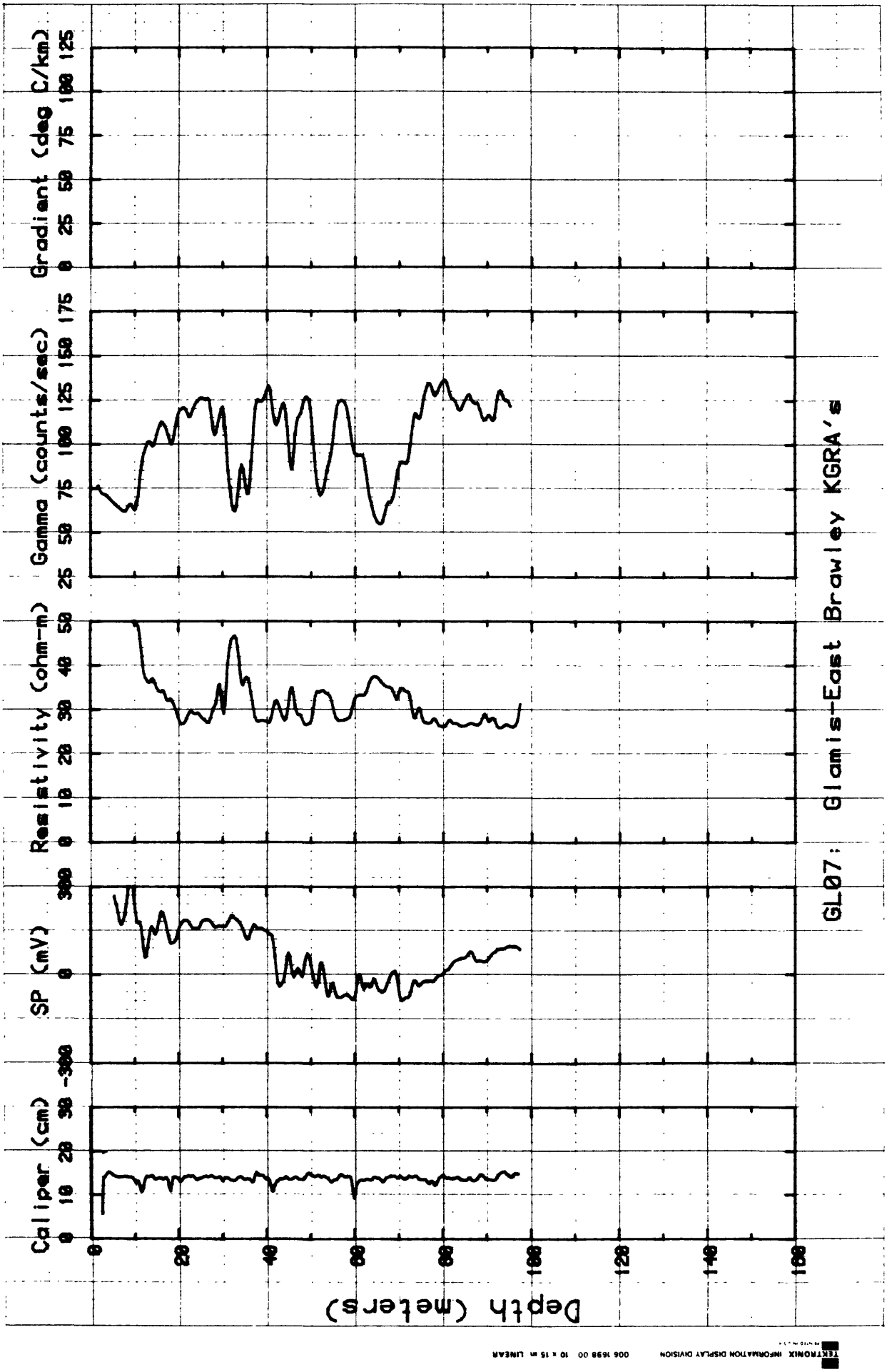

Figure III-2. Caliper, self-potential, resistivity, and gamma-ray logs for borehole GL07.

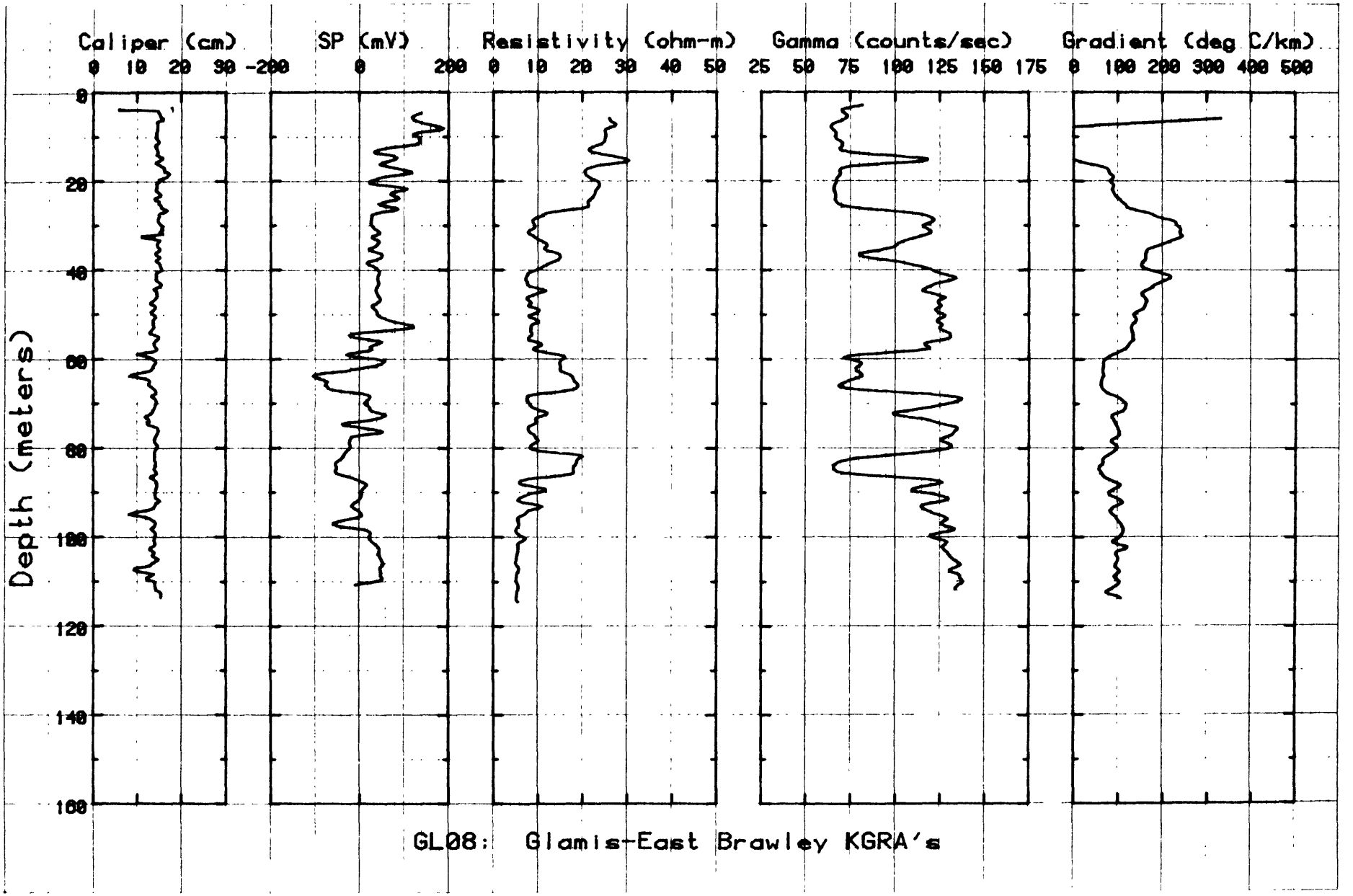

Figure III-3. Caliper, self-potential, resistivity, gamma-ray, and temperature gradient logs for borehole GL08.

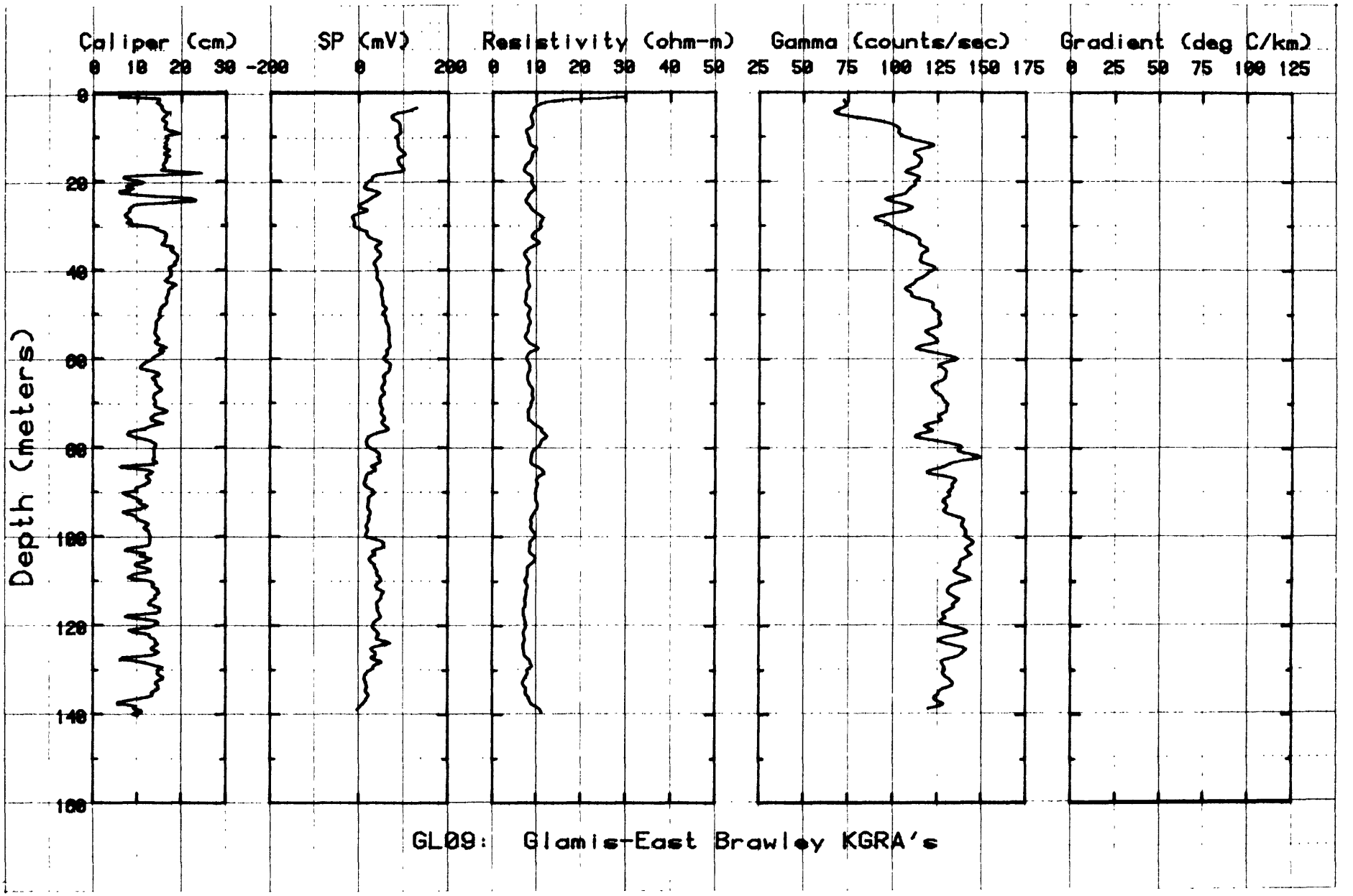

Figure III-4. Caliper, self-potential, resistivity, and gamma-ray logs for borehole GL09.

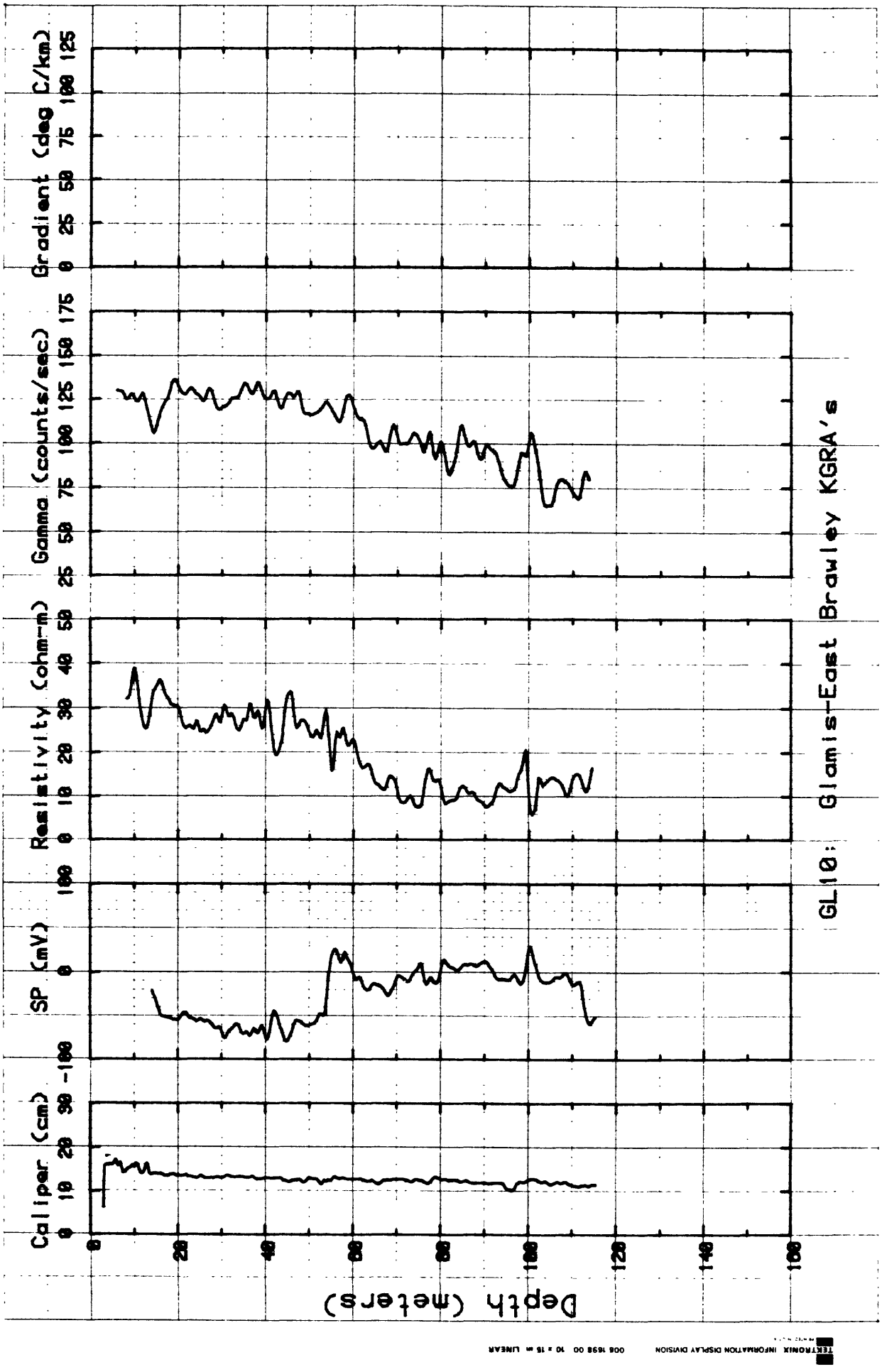

Figure III-5. Caliper, self-potential, resistivity, and gamma-ray logs for borehole GL10.

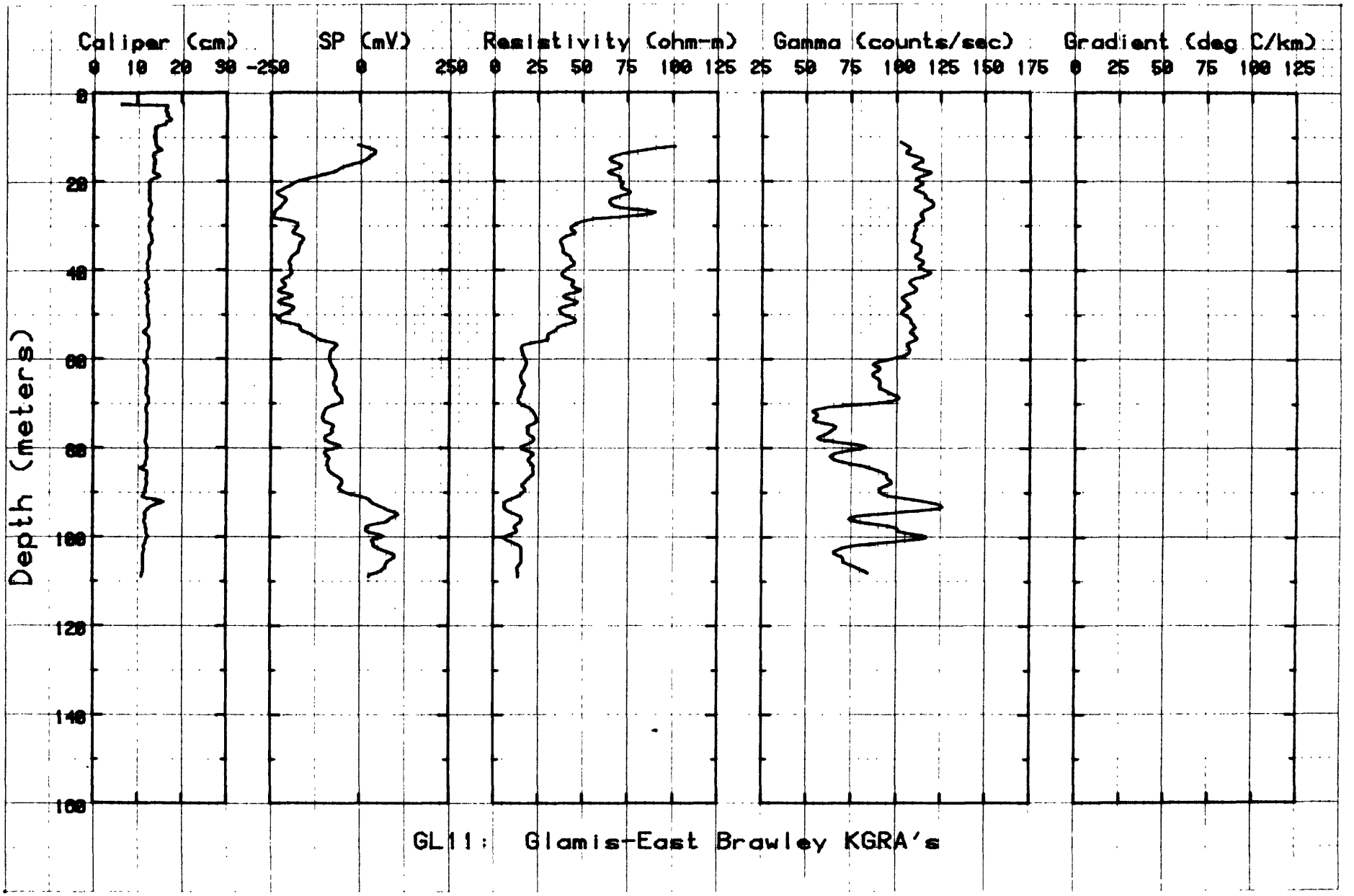

Figure III-6. Caliper, self-potential, resistivity, and gamma-ray logs for borehole GL11.

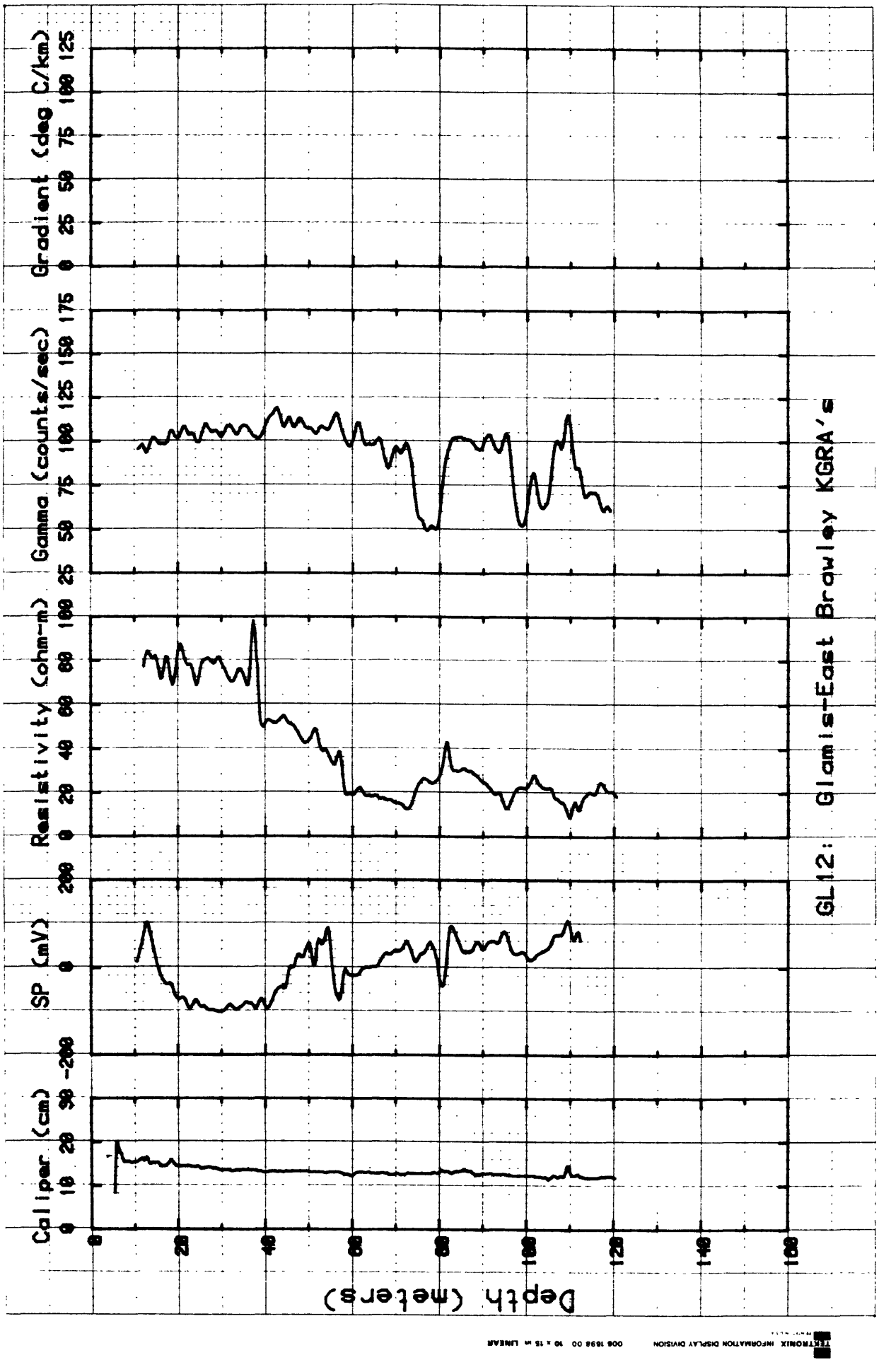

Figure III-7. Caliper, self-potential, resistivity, and gamma-ray logs for borehole GL12.

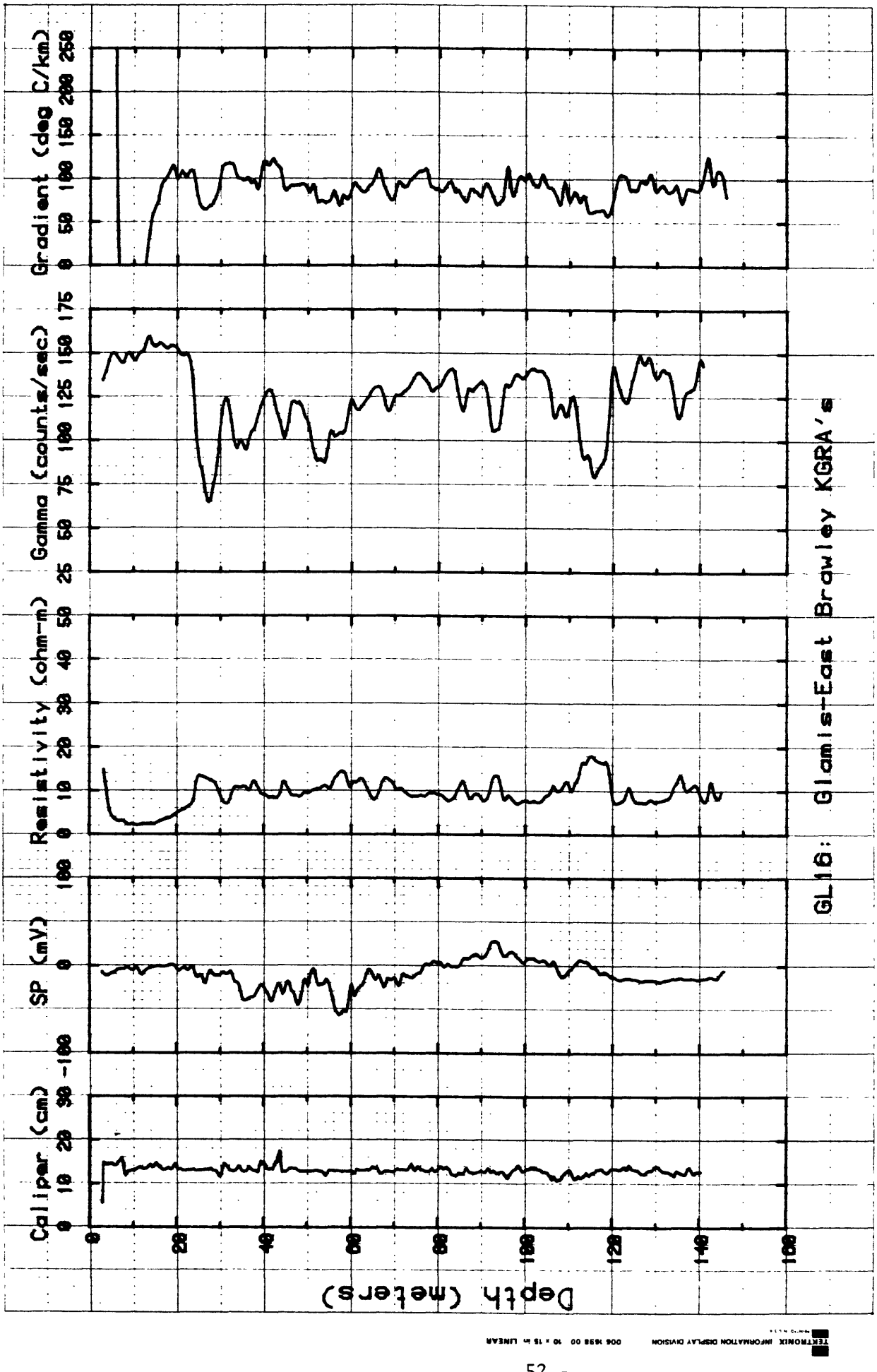

Figure III-8. Caliper, self-potential, resistivity, gamma-ray, and temperature gradient logs for borehole GL16.

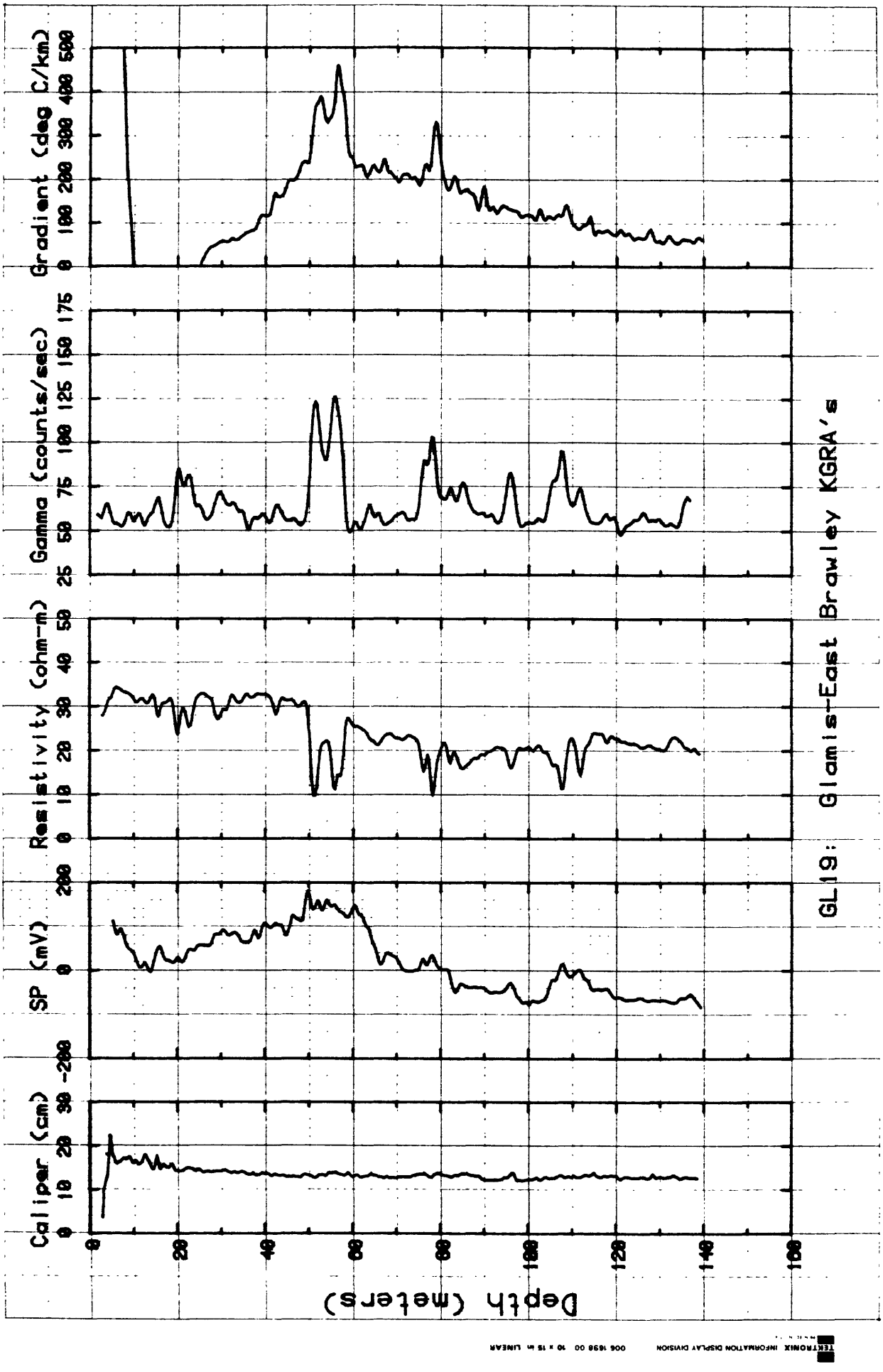

Figure III-9. Caliper, self-potential, resistivity, gamma-ray, and temperature gradient logs for borehole GL19.

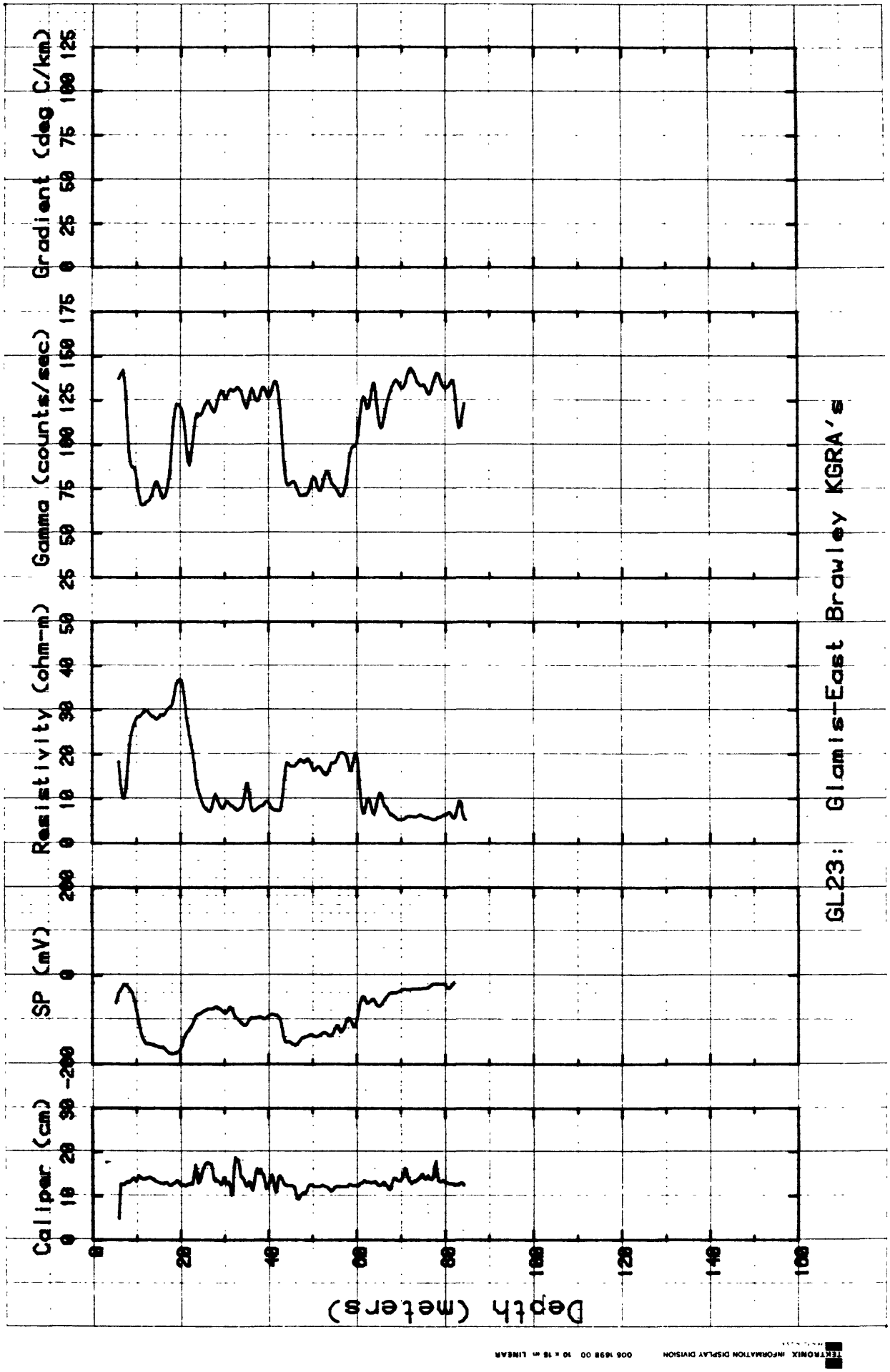

Figure III-10. Caliper, self-potential, resistivity, and gamma-ray logs for borehole GL23.

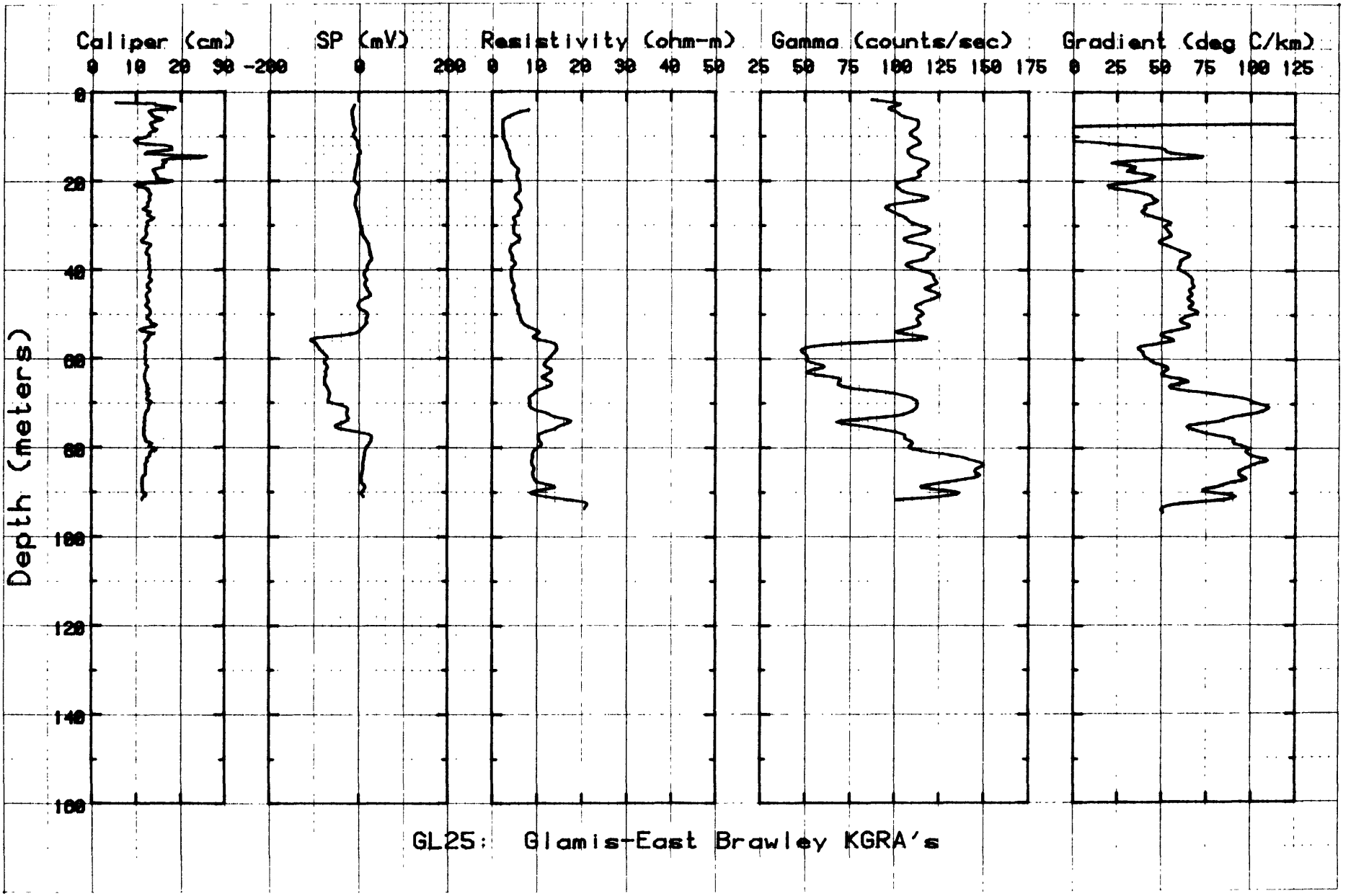

Figure III-11. Caliper, self-potential, resistivity, gamma-ray, and temperature gradient logs for borehole GL25.

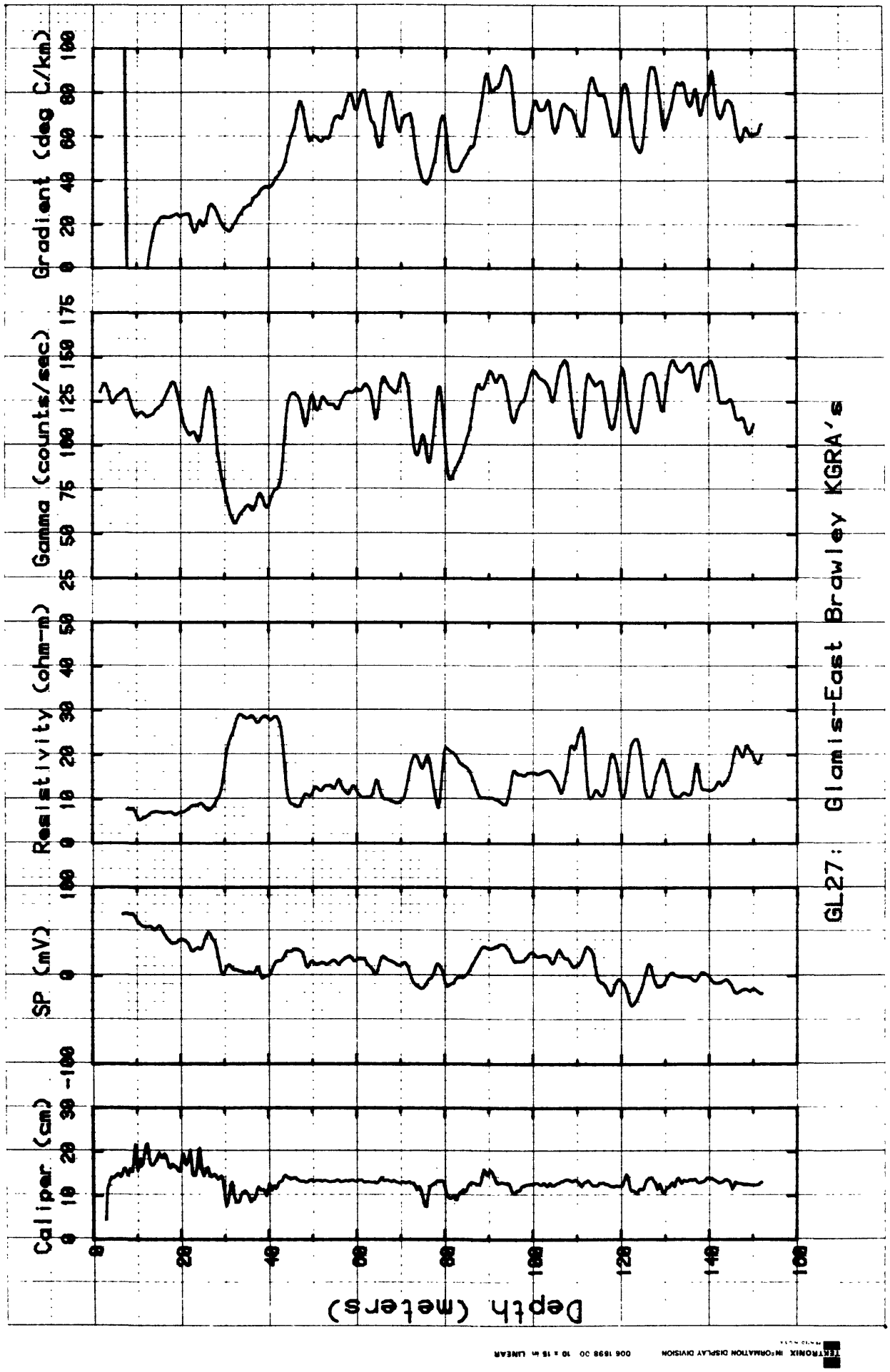

Figure III-12. Caliper, self-potential, resistivity, gamma-ray, and temperature gradient logs for borehole GL27.

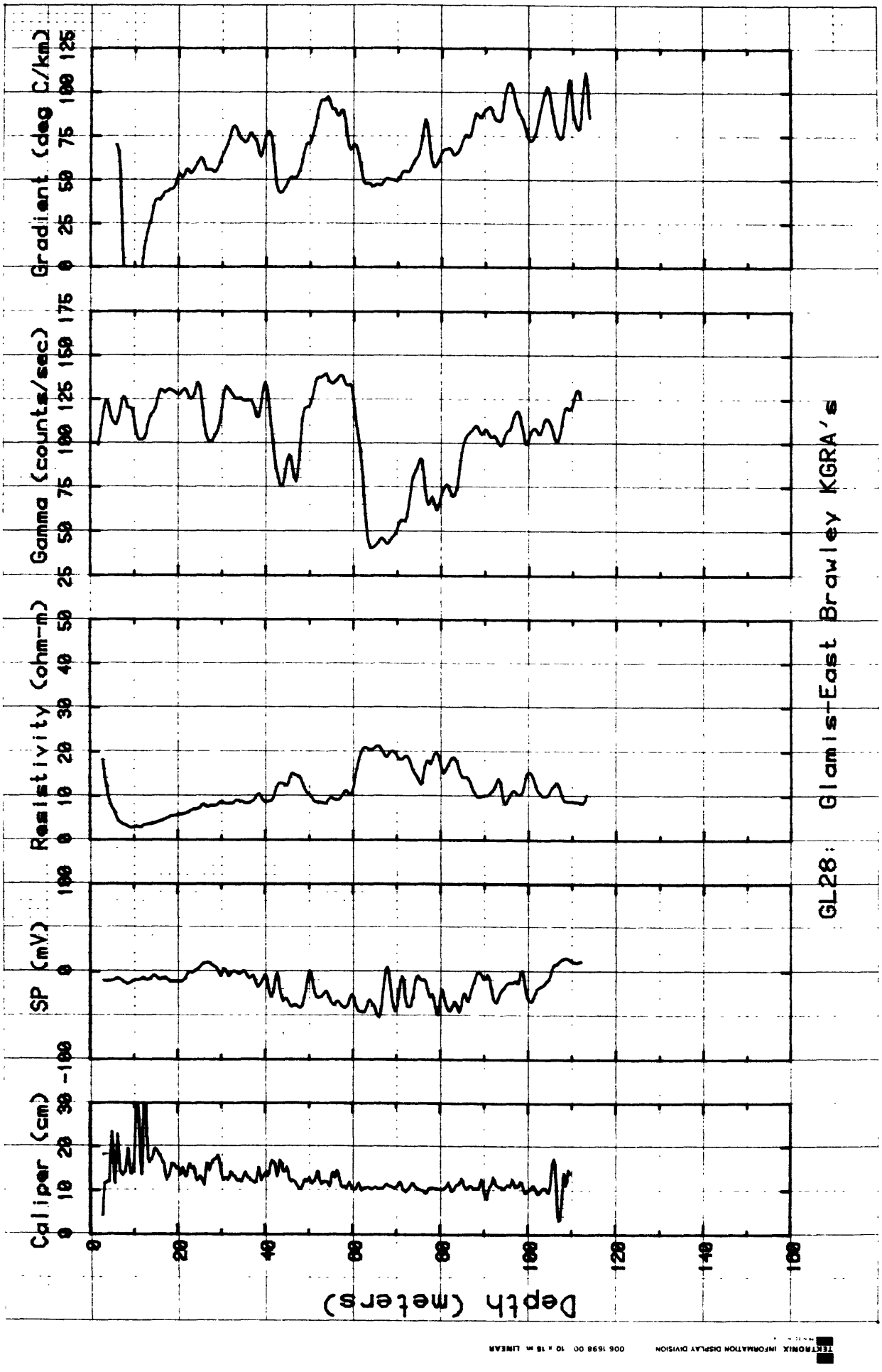

Figure III-13. Caliper, self-potential, resistivity, gamma-ray, and temperature gradient logs for borehole GL28.